

Testing aftershock models on a time-scale of decades

A. Christophersen
D.A. Rhoades

S. Hainzl
D.S. Harte

GNS Science Consultancy Report 2016/16
March 2016



DISCLAIMER

This report has been prepared by the Institute of Geological and Nuclear Sciences Limited (GNS Science) exclusively for and under contract to New Zealand Earthquake Commission (EQC). Unless otherwise agreed in writing by GNS Science, GNS Science accepts no responsibility for any use of or reliance on any contents of this report by any person other than EQC and shall not be liable to any person other than EQC, on any ground, for any loss, damage or expense arising from such use or reliance.

Use of Data:

Date that GNS Science can use associated data: March 2016

BIBLIOGRAPHIC REFERENCE

Christophersen, A.; Hainzl, S.; Rhoades, D.A.; Harte, D.S. 2016. Testing aftershock models on a time-scale of decades, *GNS Science Consultancy Report 2016/16*. 36 p.

CONTENTS

TECHNICAL ABSTRACT	II
NON-TECHNICAL ABSTRACT	IV
KEYWORDS	IV
1.0 INTRODUCTION	1
2.0 DETECTABILITY OF AFTERSHOCKS AND AFTERSHOCK DURATION	3
2.1 THE TRIGGERING TIME T	3
2.2 THE APPARENT DURATION T_A	7
2.3 THE RELATIONSHIP BETWEEN T AND T_A	9
3.0 UNIVERSAL SET OF ETAS PARAMETERS	10
4.0 THE EFFECTIVE FORECASTING PERIOD T_F	13
5.0 CONCLUSIONS AND OUTLOOK	14
6.0 ACKNOWLEDGEMENTS	16
7.0 REFERENCES	16

FIGURES

Figure 2.1	Location of 31 mainshocks from 1964 – 2011	6
Figure 2.2	Triggering time T versus background rate μ for aftershock sequences from New Zealand earthquake catalogue from 1964 for an aftershock search radius of five times the rupture length of the mainshock	7
Figure 2.3	The apparent duration T_a versus the estimated background rate for 14 New Zealand earthquake sequences with $M_{cut} = 4.0$ and search radius equal to three times the rupture length of the mainshock	8
Figure 3.1	Observed versus expected number of earthquakes of $M \geq 4.0$ for 15 New Zealand aftershock sequences within 60 days following the mainshock	11
Figure 3.2	The observed versus expected number of forecasted aftershocks in time interval 1-365 days after the mainshock for two sets of ETAS model parameters; the first was fitted to all sequences, the second was derived from physics-based models	11
Figure 3.3	The number of clusters for 224 global sequences which have more simulated aftershocks than observed	12

TABLES

Table 2.1	The location and magnitude of the mainshocks of 31 sequences in the New Zealand catalogue from 1964 – 2011, the number of events above M_4 and the estimated triggering time T in years	5
Table 2.2	The apparent duration of the Canterbury earthquake sequence calculated from Omori-Utsu law parameters determined following major earthquakes in the sequence	9
Table 3.1	Comparison of the ETAS parameters for the models in Figure 3.2	11

APPENDIX

A1.0 STATISTICAL ESTIMATION OF THE DURATION OF AFTERSHOCK SEQUENCES	19
--	-----------

TECHNICAL ABSTRACT

In New Zealand we use two aftershock models for earthquake forecasting: The Short-Term Earthquake Probability (STEP) model and variations of the Epidemic Type Aftershock Sequence (ETAS) model. These aftershock models are based on the Omori-Utsu model, a power law that describes the decay of aftershock rate with time. The models imply that aftershock activity continues for thousands if not million of years. Since homogeneous earthquake catalogues are generally available for time periods of 30 – 50 years, it is difficult to assess the validity of the aftershock models for very long time periods. This project set out to test aftershock models on a time-scale of decades. In particular, we address the following three questions:

1. For how long following a mainshock is it possible to detect aftershocks in earthquake catalogues and, in particular, how does aftershock detectability depend on the background seismicity rate?
2. How well can a universal set of ETAS parameters (constrained by physical models) forecast triggered seismicity within the observed uncertainties/variability?
3. How does the forecast ability of the ETAS model vary with an increasing time horizon¹ for individual earthquake sequences?

We use a mix of ETAS simulations and analyses of real earthquake catalogues to address the questions. For our analyses, we distinguish three different time scales of aftershock activity: (1) the triggering time T , which is the duration of the physical triggering process of a single event; (2) the apparent aftershock duration T_a which is the time period in which aftershocks dominate the seismicity; and (3) the effective forecasting period T_f within which earthquake rate estimates are significantly improved by time-dependent seismicity models after a large earthquake.

A finite value of T is expected from a physical point of view, but has not been incorporated in standard ETAS model applications so far. During this project we introduce and estimate for the first time finite T -values in the modified ETAS model.

Although estimates of T were only weakly constrained and potentially subject to biases due to limited catalogue length and cluster selection, our comparative analysis of synthetic sequences gave some robust results: We found that T has an impact on the estimates of the other ETAS-parameters and reduces the mismatch between the power law decay parameter in the ETAS model and predictions of physics-based models. Furthermore, the predicted inverse proportionality between T and the background rate is in agreement with the observed trend in the estimated values of T for empirical earthquake sequences.

We estimated T_a for all earthquake sequences with at least 50 earthquakes in our three different earthquake catalogues, as well as for simulated sequences. We found that many sequences had durations T_a of less than one year and only few lasted longer than 10 years. This finding contradicts our current aftershock models. We have suggested two ways of changing the models but pursuing these is outside the scope of this EQC project.

¹ The time horizon here mean the time into the future for which an earthquake forecast applies. We later refer to this as “effective forecasting period T_f ” within which earthquake rate estimates are significantly improved by time-dependent seismicity models after a large earthquake.

Our forecast experiment with universal ETAS parameters confirmed earlier work that universal ETAS parameters do not fit all sequences well. However, estimating parameters for an on-going sequence has too many uncertainties and does not lead to stable results. It was outside the scope of this project to investigate what universal set of parameters might be best.

The effective forecasting period T_F depends on several factors, including (1) the number and quality of data available; (2) the quality of the model, i.e. how well the model describes the observed seismicity and (3) the magnitude difference between mainshock and cut-off magnitude. We conducted a numerical experiment of ETAS simulations and found that after approximately 100 days for $M = 6$ and 1000 days for $M = 7$, the forecast of the time-invariant Poisson model becomes equal to or better than that of the modified ETAS model.

In summary, our project on “Testing aftershock models on time-scale of decades” answered the three questions posed above. We found that many aftershock sequences cannot be detected above the background seismicity for more than 1 year, and only few sequences last longer than 10 years. A universal set of ETAS parameters does not fit all earthquake sequences well, but fitting the parameters to individual sequences introduces many uncertainties. Finally, the effective forecasting time of the ETAS model is only in the order of 100 and 1000 days for mainshocks of $M6$ and $M7$, respectively.

NON-TECHNICAL ABSTRACT

Aftershocks are the smaller earthquakes that normally follow a larger earthquake, the so-called mainshock. The frequency of aftershock decays with time from the mainshock. We use aftershock models for earthquake forecasting that mathematically describe this decay. According to these models, aftershock activity can continue for years, even thousands of years. Earthquakes that occur outside a mainshock-aftershock sequence are called background seismicity.

We investigate three questions regarding aftershock occurrence:

1. How long can we detect aftershocks before they merge with the background seismicity?;
2. Can a single set of model parameters in our aftershock models describe all aftershock sequences well?; and
3. For how long following a mainshock can we forecast aftershocks accurately?

We found that the duration of an aftershock sequence, i.e. the time before it aftershocks merge with the background seismicity, is difficult to determine. It depends on both the background seismicity and the mainshock magnitude, and can vary from a few days to many years. In New Zealand, the longest duration was found for the Canterbury sequence because the background seismicity was very low prior to the 2010 Darfield earthquake.

In response to the second question, we found that a single set of aftershock parameters did not describe all aftershock sequences well. However, the alternative approach of fitting individual sequences had many uncertainties, and unfortunately did not necessarily provide better results than using a uniform set of model parameters.

To address the third question, we conducted a numerical experiment where we created synthetic earthquake catalogues based on one of our aftershock models. We found that the time in which aftershock models can effectively forecast earthquakes of magnitude 4 and larger was only about 100 or 1000 days after a mainshock of magnitude 6 or 7, respectively.

KEYWORDS

Aftershock models, Omori-Utsu law, duration of aftershock sequences

1.0 INTRODUCTION

This project set out to test aftershock models on a time scale of decades. Generally aftershocks are understood to be triggered by a larger earthquake, the mainshock. Their rate decays quickly in the days and weeks following the mainshock. The decay of aftershock rate is described by the Omori-Utsu law (Equation 1 in the appendix), which has a decay parameter p (Utsu et al., 1995). Generic parameters for the Omori-Utsu law derived from New Zealand aftershock sequences (Pollock, 2007) suggest that it takes nearly 800 days for half of the aftershocks to occur, and more than a million years for 80% of the aftershocks to occur. Thus a large percentage of earthquakes that we observe could be seen as aftershocks of mainshocks that occurred thousands if not millions of years ago.

The 1891 Nobi Japan aftershock sequence that led Omori to propose the power-law decay (Omori, 1894) was found to be still obeying the law after 100 years with the decay parameter $p=1.0$ (Utsu et al., 1995). Homogeneous earthquake catalogues are generally available for time periods of 30 – 50 years, and therefore it is difficult to assess the validity of the Omori-Utsu law for very long time periods. As a first step in our project we want to investigate how long after a mainshock aftershocks can be detected. Since there is nothing unique about an aftershock compared to any other earthquake, we need to define a model to help us decide whether an earthquake is an aftershock or not.

Two aftershock models are currently used in New Zealand: The Short-Term Earthquake Probability (STEP) model (Gerstenberger et al., 2004; Gerstenberger et al., 2005) and variations of Epidemic Type Aftershock Sequence (ETAS) model (Harte, 2013; Ogata, 1988; Rhoades, 2013). These aftershock models are based on the Omori-Utsu law. For the STEP model, the Omori-Utsu law parameters are determined for an entire aftershock sequence, and thus the parameter p represents the decay of the whole sequence. The ETAS model assumes that each earthquake, including each aftershock, triggers its own family of aftershocks. The Omori-Utsu law parameters are fitted to the cascading sequences, and the decay parameter applies to the direct aftershocks of a single earthquake. In New Zealand the generic p for STEP is 1.07 (Pollock, 2007) and for ETAS 1.17 (Harte, 2013). The smaller the p -value, the slower an aftershock sequence decays. A value of p less or equal to 1.0 in the Omori-Utsu law implies that the number of aftershocks becomes infinite with time. By contrast, physical models for aftershock decay postulate p to be less or equal to 1.0 and have a finite triggering time T , which is the latest possible time for an earthquake to trigger and aftershock (Dieterich, 1994; Dieterich et al., 2000; Helmstetter and Shaw, 2006).

During this EQC project, we introduce for the first time a finite triggering time into the ETAS model by truncating the Omori-Utsu law. This mimics the finite triggering times in physics-based models and allows for smaller values of the decay parameter p . We simulate earthquake catalogues with finite triggering times of 100 and 1,600 days, and then fit the conventional ETAS model with infinite triggering time. This will help us understand the effect of a finite triggering time T on the ETAS model parameter, and possibly shorten the very long theoretical duration of aftershock sequences.

Aftershock models play an important role in the seismic hazard modelling for the recovery of Christchurch. Following the devastating 2011 Christchurch earthquake GNS Science led the development of the time-varying Canterbury seismic hazard model (Gerstenberger et al., 2014). The earthquake rate model is a hybrid model combining four-time varying and four time-invariant earthquake rate models. The weight given to each individual model was

determined by an expert elicitation procedure. Two aftershock models, a version of STEP and a version of ETAS, received 36% and 19% respectively. The remaining 45% for the time-varying models was about equally split between two versions of the 'Every Earthquake a Precursor According to Scale' (EEPAS) model (Evison and Rhoades, 2004; Rhoades and Evison, 2004; Rhoades and Evison, 2005). Contrary to the aftershock models that describe the decay of seismicity following a large earthquake, EEPAS uses the increase in small earthquake prior to large earthquakes to forecast future large earthquakes.

EQC project BIE 12/633 funded the retrospective test of the operational hybrid forecast model for Canterbury (Rhoades et al., 2013). The results have recently been published (Rhoades et al., 2016). One key finding was that all models underpredicted the number of earthquakes in the testing period. This was due to an abnormally large number of earthquakes in the period starting with the Dusky Sound earthquake in 2009 and continuing with the Canterbury sequence. The second finding was that hybrid models performed better than any individual model. A new hybrid model that optimised the contributions from the individual models gave nearly no weight to the aftershock models. The last finding justifies further investigating the aftershock models. In particular, we proposed to address the following three questions:

1. For how long following a mainshock is it possible to detect aftershocks in earthquake catalogues and, in particular, how does aftershock detectability depend on the background seismicity rate?
2. How well can a universal set of ETAS parameters (constrained by physical models) forecast triggered seismicity within the observed uncertainties/variability?
3. How does the forecast ability of the ETAS model vary with an increasing time horizon for individual earthquake sequences?

These questions are very challenging, and unfortunately it is not possible to do full justice to all of them within the constraints of this project. We have done extensive simulations as well as real earthquake catalogue analyses to answer questions 1 and 3. The results have been submitted to Geophysical Journal International. The revised and accepted manuscript 'Statistical estimation of the duration of aftershock sequences' is included in the Appendix. Question 2 was not investigated in as much detail as we would have liked. However, with some of our own simulations, as well as referring to the literature, we have been able to come to some solid conclusions. In the following three sections we address each of the questions, referring where appropriate to the manuscript. The report closes with conclusions and an outlook in Section 5.

2.0 DETECTABILITY OF AFTERSHOCKS AND AFTERSHOCK DURATION

Our current aftershock models have no finite triggering time and, due to the power law decay of aftershock rate, aftershocks can continue for a very long time. Therefore it is worthwhile to explore for what time period we can detect aftershocks in the earthquake catalogue. There is nothing unique distinguishing an aftershock from any other earthquake, and for that reason we need a model to help us to classify aftershocks. We used two statistical approaches. First, we introduced a finite triggering time T in the ETAS model by truncating the Omori-Utsu law. This mimics the finite duration in physics-based models during which it is possible for an earthquake to trigger an aftershock. In the second approach, we looked at the overall aftershock decay following a mainshock and defined an apparent aftershock duration T_a as the time when the Omori-Utsu aftershock rate is equal to the background seismicity prior to the mainshock. In both cases we worked with simulated catalogues first, and then analysed one global earthquake catalogue and the regional earthquake catalogues for New Zealand and California. The method and results using both approaches are presented in Sections 4 and 5 in the Appendix. Below we summarise the key points and show some results specific to New Zealand.

2.1 THE TRIGGERING TIME T

We introduced an additional parameter T into the ETAS model, which is the maximum time interval over when an earthquake can trigger direct aftershocks. In practice this involves the truncation of the Omori-Utsu law at time T . We simulated earthquake catalogues with T -values of 365, 1000, and 10,000 days and durations of 30 years to have comparable data to the real catalogues. Section 4 in the Appendix describes the simulations in detail. Figure 4 in the Appendix shows the estimated T versus the estimated background rate for these simulated catalogues. Triggering times up to $T=1000$ days could be recovered, while triggering times of 10,000 days, i.e. in the order of the catalogue length, were almost unconstrained. The uncertainty in fitting the data increased with increasing triggering time T .

When we fitted the ETAS model with finite triggering time T to the real catalogues, we found that the estimated T ranged from a few days to the duration of the catalogue. Figure 2a in the Appendix shows the frequency distribution of the estimated triggering time T for empirical sequences from the real catalogue data. Figure 2b shows the estimated triggering time T versus mainshock magnitude, and gives the impression that these two parameters are not correlated. Both plots illustrate the large scatter when estimating the triggering time T .

We also investigated the relationship between triggering time T and the background seismicity. Figure 5 in the Appendix shows the estimated triggering time for the real catalogues as a function of (a) the estimated background rate of $M \geq M_{\text{cut}}$ events per day, and (b) the estimated background rate density, defined as the number of $M \geq 0$ events per day and per km^2 . The scatter in plot (b) is slightly reduced since all earthquake sequences are scaled to the same minimum magnitude. The results indicate a tendency for the triggering time T to be inversely proportional to the background rate density. While the signal is weak, it is consistent with forecasts of the rate-and-state dependent frictional response of fault networks to mainshock-induced static stress changes (Dieterich, 1994) as further explained in Section 4 of the Appendix.

Table 2.1 lists the location and magnitude of the mainshocks of 31 sequences in the New Zealand catalogue from 1964 – 2011, which are found by the clustering algorithm with a search radius of five times the rupture length. The table includes the name and time of the mainshock, the number of events in the sequence and the estimated triggering time T in years. Figure 2.1 shows a map where the location of the mainshock is marked with the cluster number from Table 2.1. Surprisingly, there is no correlation between the triggering time T and the location of the sequences. For example, cluster 6, 8, and 18 occurred in the Buller ranges with triggering times ranging from just over 100 days to nearly 20 years (highlighted in yellow in Table 2.1). It is not clear whether sequences within close vicinity actually have such different triggering times T , or whether the variation is due to uncertainties in parameter estimation.

Figure 2.2 illustrates the uncertainties in the estimation of the triggering time T by showing the relationship between triggering time T and the background rate for the data in Table 2.1 and Figure 2.1. The confidence intervals indicate the large uncertainties in T estimates. Green lines in the figures indicate a $1/\mu$ relationship while the magenta coloured lines show the least-squares fit of T_a versus μ . The correlation between the two parameters is weak, possibly due to the uncertainty in parameter estimates. However, the trend is consistent with physical models.

Table 2.1 The location and magnitude of the mainshocks of 31 sequences in the New Zealand catalogue from 1964 – 2011, the number of events above M4 and the estimated triggering time T in years. The yellow lines highlight sequences near the 1968 Inangahua earthquake, which occurred about 24 km to the west of the 1929 M7.6 Buller earthquake.

Cluster number	Name/location	Date of mainshock	M _L	Latitude	Longitude	Number of events M≥4.0	T [years]
1	Milford Sound	08.03.1964	5.77	-44.19	167.60	96	22.92
2	Kaikoura	11.04.1965	6.14	-42.76	174.14	75	1.64
3	Bay of Plenty	15.06.1965	5.79	-37.81	177.55	71	23.56
4	Gisborne	04.03.1966	5.98	-38.74	178.11	166	0.03
5	Cook Strait	23.04.1966	5.83	-41.64	174.54	136	0.12
6	1968 Inangahua	24.05.1968	6.7	-41.76	172.04	687	2.76
7	Southland	25.09.1968	5.91	-46.53	166.57	113	8.68
8	Buller Ranges	13.08.1971	5.83	-42.08	172.15	78	19.50
9	Fiordland	21.09.1974	5.54	-44.34	168.05	76	0.02
10	Taranaki	05.11.1974	5.95	-39.54	173.46	51	2.30
11	Weber	10.06.1975	5.76	-40.31	176.07	95	4.26
12	Milford Sound	04.05.1976	6.55	-44.67	167.38	1137	1.59
13	Cook Strait	18.01.1977	6.01	-41.84	174.58	132	0.11
14	Lake Tekapo	24.06.1984	5.93	-43.59	170.63	58	0.22
15	Edgecumbe	02.03.1987	6.08	-37.89	176.80	186	0.25
16	Te Anau	04.06.1988	6.07	-45.33	166.87	821	2.16
17	Weber	13.05.1990	6.25	-40.43	176.47	187	0.05
18	Buller Ranges	29.01.1991	6.29	-41.90	171.73	76	0.35
19	Weber	02.03.1992	5.75	-40.43	176.60	75	4.26
20	Arthur's Pass	30.03.1992	5.77	-43.04	171.23	139	11.23
21	White Island	21.06.1992	6.14	-37.58	176.87	244	0.24
22	Secretary Island	10.08.1993	6.7	-45.21	166.71	1114	1.98
23	Arthur's Pass	18.06.1994	6.67	-43.01	171.48	638	1.44
24	Arthur's Pass	24.11.1994	6.29	-42.95	171.82	300	1.05
25	Secretary Island	01.00.2000	6.23	-45.12	166.95	577	0.27
26	Haast, West Coast	08.12.2001	6.16	-44.11	168.61	54	0.58
27	Fiordland	22.08.2003	6.99	-45.19	166.83	801	1.98
28	George Sound	15.10.2007	6.74	-44.74	167.44	248	0.82
29	Gisborne	20.12.2007	6.71	-38.89	178.54	67	0.26
30	Dusky Sound	15.07.2009	7.8	-45.77	166.59	834	2.46
31	Darfield, Canterbury	04.09.2010	7.1	-43.53	172.17	429	1.11

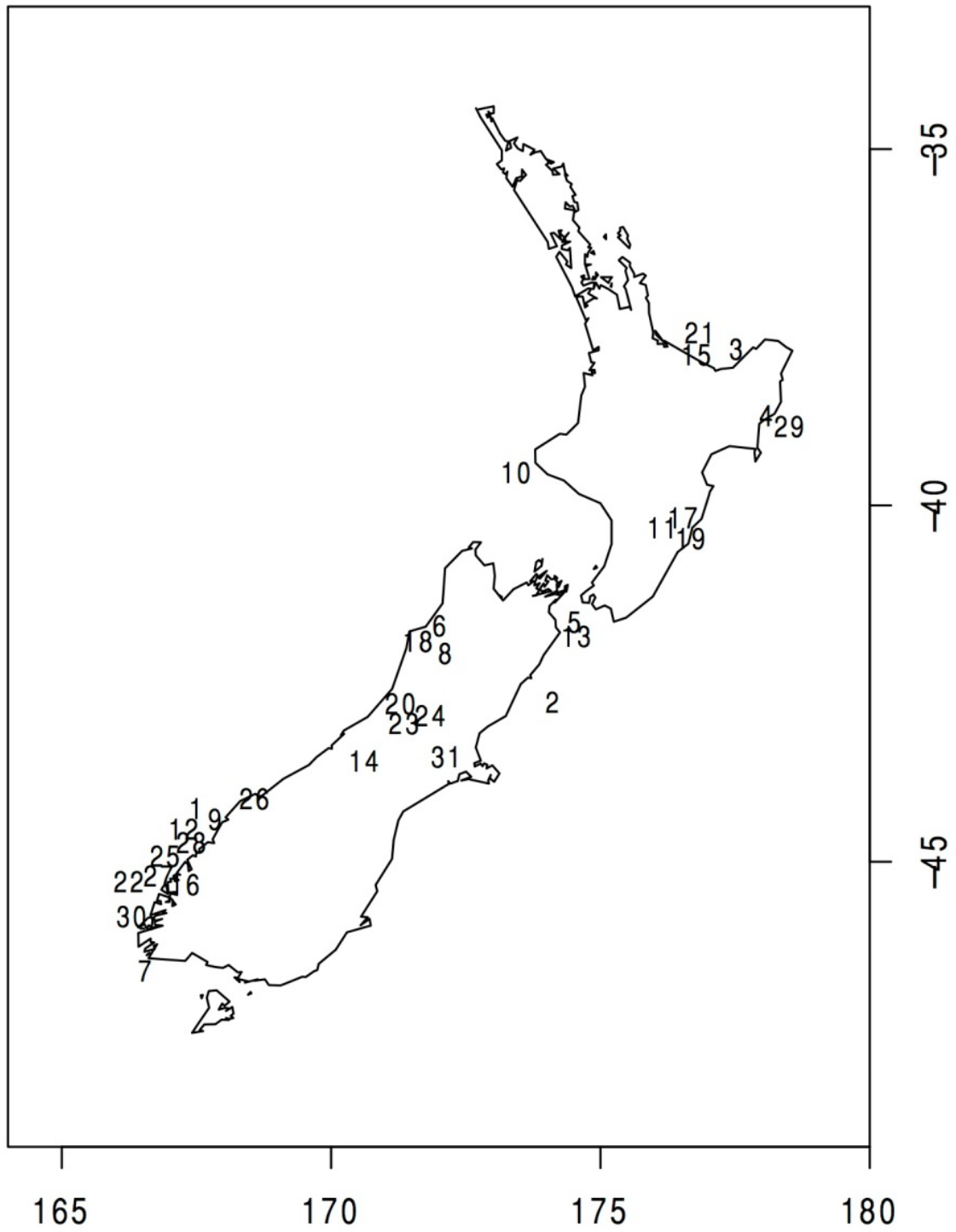


Figure 2.1 Location of 31 mainshocks from 1964 – 2011. Please refer to Table 2.1 for more details.

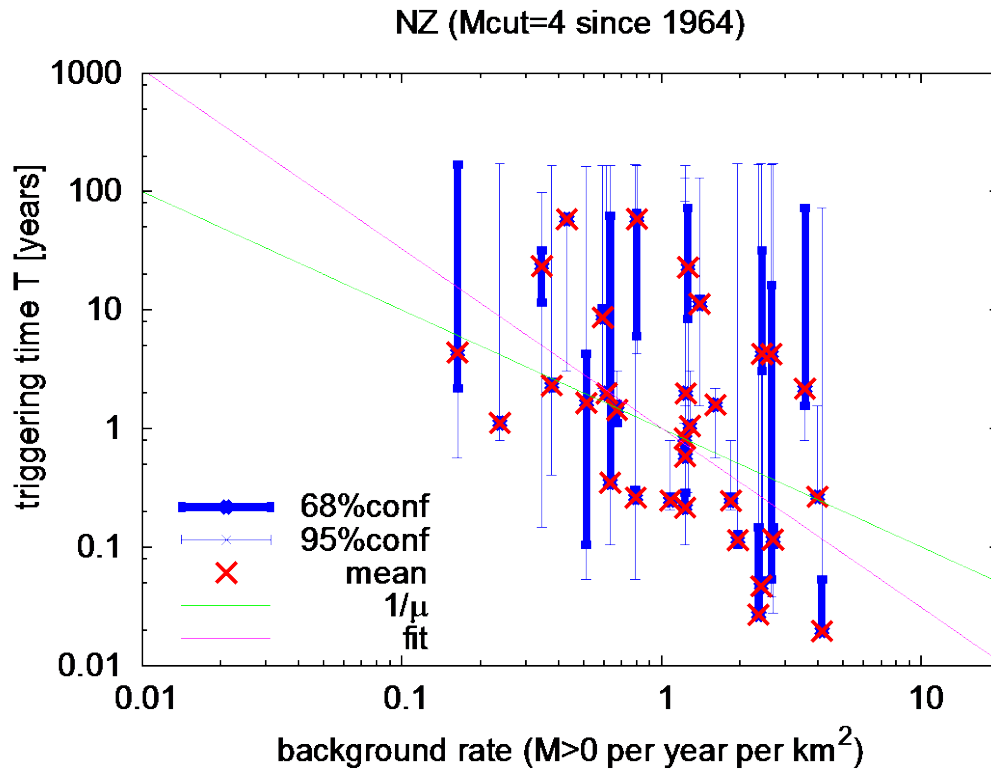


Figure 2.2 Triggering time T versus background rate μ for aftershock sequences from New Zealand earthquake catalogue from 1964 for an aftershock search radius of five times the rupture length of the mainshock.

2.2 THE APPARENT DURATION T_a

We define the apparent duration T_a as the time period over which the seismicity rate from aftershocks is larger than the background seismicity. Thus we can calculate T_a as the elapsed time after the mainshock at which the overall decay of the Omori-Utsu law is equal to the background rate μ . For each mainshock, we have estimated the parameters μ , K_0 , c , p describing the Omori-Utsu rate $R(t) = \mu + K_0 (t + c)^{-p}$ by means of maximum likelihood estimation. We used one year prior to the mainshock to estimate the background rate μ , and one year following the mainshock to estimate the Omori-Utsu parameters. We note that these parameters take the effects of secondary and higher order aftershocks into account, in contrast to the results of the ETAS model application where parameters are related to aftershocks directly triggered by one mother event. The inverted parameters are then used to estimate T_a by the condition that $R(T_a) = 2\mu$, that is, the aftershock rate equals the background rate.

It is challenging to automatically estimate T_a in this way due to the clustering of earthquakes that is not detected with this simplified method. Clustering in the time before the mainshock can lead to an increase of the estimated background rate and thus to a shortening of T_a . Choosing a larger search radius increases the chance of including unrelated earthquake clusters. However, choosing too small a search radius may lead to no background earthquakes being found. We reduced the search radius from five to three times the rupture length of the mainshock because the larger area seemed to pick up too much unrelated seismicity that this simple model could not distinguish as potential clustering.

Large aftershocks can trigger their own aftershock decay. Again, this simplified model cannot detect secondary clustering, leading to a lower p-value as demonstrated for the Canterbury sequence (Christophersen, et al., 2013). A lower p-value means a longer decay and thus longer apparent duration T_a . We therefore calculated the apparent duration with the fitted p-value and with a fixed p-value of 1. Figure 2.3 shows the apparent duration T_a versus the estimated background rate with the crosses showing the results with the fitted decays parameter p and the dots the results from a fixed decay parameter p of 1. The Darfield earthquake has the longest apparent duration of around 3,900 days (around 10 years) for the fitted parameters (highest cross in the plot). T_a is reduced to around 1,100 days (less than three years) with a fixed decay parameter of 1.0. This duration seems too short, and the background seismicity in the middle of the data for all of New Zealand seems too high. Therefore we have repeated the calculation with data we determined earlier. For the area of the current Canterbury earthquake forecast (longitude 171.6E – 173.2E and latitude 43.9S – 43.3S) we found that the background rate was 0.24 $M \geq 4.0$ earthquakes per year in the time period 1964 – 2009, and 5.1 $M \geq 3.0$ earthquakes per year in the time period 1987 - 2009. Table 2.2 lists the fitted Omori law parameters from a previous EQC report for the Canterbury sequence, following the Darfield, Christchurch and June 2011 earthquakes, as well as the resulting duration. For the aftershocks following the Darfield and the Christchurch earthquakes this method of estimating apparent duration T_a suggests that the overall sequence will last just under 40 years. The apparent duration T_a increases to 92 years following the June 2011 earthquakes. However, this is likely to be an artefact of the low decay parameter $p=0.77$.

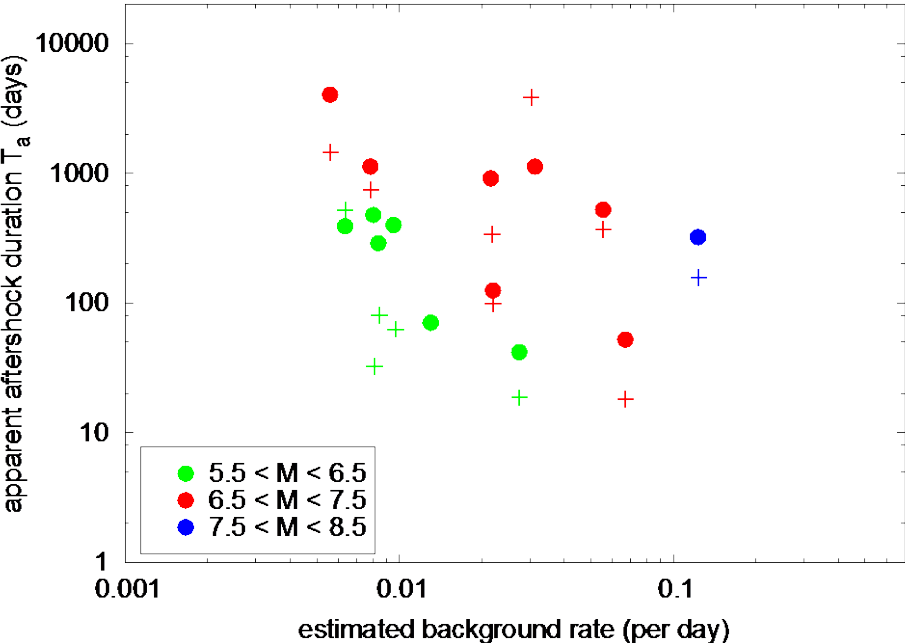


Figure 2.3 The apparent duration T_a versus the estimated background rate for 14 New Zealand earthquake sequences with $M_{cut} = 4.0$ and search radius equal to three times the rupture length of the mainshock. The crosses show the results with the fitted decay parameter p and the dots the results from a fixed decay parameter p of 1.

Table 2.2 The apparent duration of the Canterbury earthquake sequence calculated from Omori-Utsu law parameters determined following major earthquakes in the sequence

Earthquake	background $M \geq 3.0$ [years] from 1987 - 2009	c [days]	p	K_0	T_a [years]
Darfield	5.1	0.112	1.03	261.4	38
Christchurch	5.1	0.035	0.94	112.7	39
June 2011	5.1	0.001	0.77	42.6	92

Our EQC proposal posed the question whether the 1968 ML 6.7 (Mw 7.2) Inangahua earthquake was an aftershock of the 1929 ML 7.3 (Mw 7.8) Murchison earthquake. Table 2.1 shows that cluster 6, 8, and 18 occurred in the Buller ranges with triggering times T ranging from just over 100 days to nearly 20 years (highlighted in yellow in Table 2.1). The apparent duration T_a for any of these sequences with different cut-off magnitudes and search radii was never larger than 6 years. This could be underestimated due to on-going aftershock activity. However, given the challenge in distinguishing aftershocks from the background seismicity, we did not pursue this question any further during the project.

2.3 THE RELATIONSHIP BETWEEN T AND T_a

The apparent duration T_a is not necessarily related to the triggering time T . In Section 5 in the Appendix we used the ETAS model with a finite triggering time T of 1,000 days to simulate aftershock sequences with mainshock magnitude and different background seismicity. We then applied the method of Section 2.2 to estimate T_a . The results are shown in Figure 6a of the Appendix. It is obvious that the estimate of T_a is strongly dependent on the mainshock magnitude and inversely proportional to the background rate, while the triggering time is in all cases the same ($T = 1000$ days). Thus T_a and T are quite different quantities.

Although T_a and T are almost independent quantities, T_a is related to how well the estimation of the triggering time T is constrained. The estimation of T is better constrained for sequences with significant on-going aftershock activity at time T , that is, in the case of large T_a . If T_a is estimated from first aftershocks, as done here, this means that T - estimates are expected to be well constrained for $T_a \geq T$. As shown above, T_a depends on the mainshock magnitude and the background rate. Thus T can be best estimated for large mainshocks and low background rates.

3.0 UNIVERSAL SET OF ETAS PARAMETERS

Various applications of the ETAS model on different data sets have indicated strong variations of the parameter estimates in space and time. However, such apparent variations can be partly related to the large uncertainties due to catalogue incompleteness, inappropriate modelling of the spatial aftershock distribution, and presence of aseismic forcing (Hainzl, 2013; Hainzl et al., 2008; Hainzl et al., 2013; Harte, 2013). Harte (2013) fitted a series of ETAS models to the New Zealand earthquake catalogue, and then applied the best-fitting parameter set to 15 aftershock sequences. Figure 3.1 shows the observed versus the expected number. The expected number was calculated by applying the ETAS rate function (similar to Equation 2 in the Appendix but with an additional spatial term) to each earthquake in the sequence for 60 days from the mainshock and integrating the rate function over time and all earthquakes. This is a retrospective test of how well the ETAS model described the data. Except for one sequence, all sequences had more earthquakes than predicted by the ETAS model. In contrast, the ETAS model predicted more earthquakes to occur in areas outside active aftershock sequences than were observed there (Harte, 2013). When fitting the 15 sequences individually, only six had ETAS parameters that were stable. The number of earthquakes per sequence ranged from 16 – 851 and there was no correlation between the number of events in a sequence and whether the fitted ETAS parameters were reasonable. This again seems to be caused by the large uncertainty in parameter estimation, and is an indication that even up to 850 aftershocks may not be enough to get stable results. Furthermore, the results were obtained from the finalised earthquake catalogue. Fitting the ETAS parameters to provisional earthquake catalogue from an on-going earthquake sequence would be even more unstable due to data quality issues. Thus we conclude that while a single set of ETAS parameters derived from fitting the complete earthquake catalogue did not fit all sequences well, the fitting of individual sequences often leads to unstable results.

To understand the performance of a single set of parameters for all aftershock sequences, we undertook a forecasting experiment with two different sets of ETAS parameters. The first set was derived by fitting the ETAS parameters to all 224 sequences in the global data set (See section 2.2 in the Appendix for details on the data and the cluster selection). The second set used physics-based models for some parameters. Table 3.1 compares the two sets of parameters. Figure 3.2 shows the observed versus expected number of aftershocks from day 2 to day 365 for the two sets. The expected number of aftershocks was calculated by taking the mainshock and aftershocks on the first day as input history for the ETAS model and then averaging the number of aftershocks from 1000 simulations of day 2 – 365. The difference between the local regression and the best fit line illustrates the sensitivity to some outliers with large differences between the observed and expected number. In particular, the 2004 M9.1 Sumatra earthquake with 865 $M \geq 5.0$ aftershocks from day 2 – 365, had less than 500 expected earthquake with the ETAS parameters fitted from the data but 900 with the physics based parameters. Comparison of the equality line with the linear model fit in Figure 3.2 indicates that the expected number is systematically larger than the observed number. This is the opposite result compared to the New Zealand example in Figure 3.1.

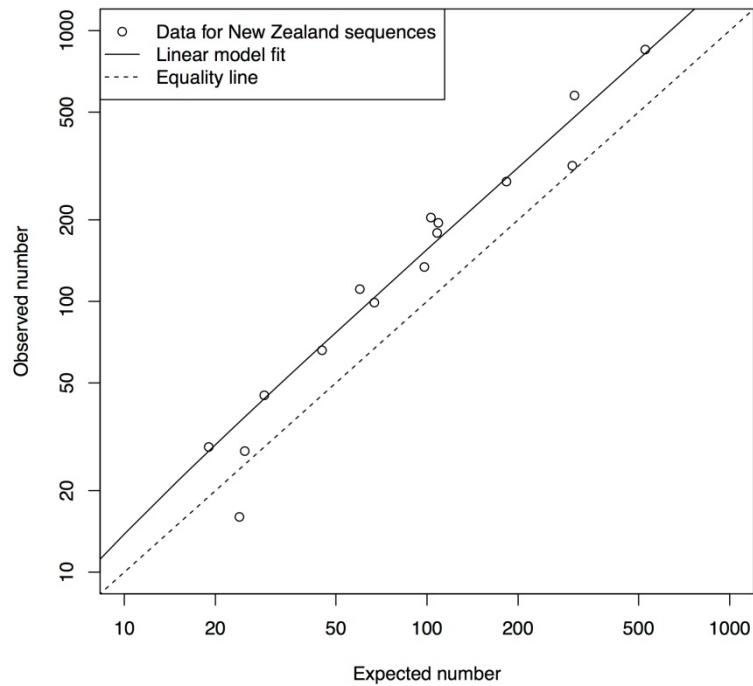


Figure 3.1 Observed versus expected number of earthquakes of $M \geq 4.0$ for 15 New Zealand aftershock sequences within 60 days following the mainshock.

Table 3.1 Comparison of the ETAS parameters (see equation 2 of the Appendix) for the models in Figure 3.2. In both cases, the minimum and maximum magnitude are 5.0 and 9.5, respectively. The b -value is fitted to all data as 1.07, and thus the α -value is chosen to be the same for the physics-based parameters. A finite triggering time T of 10,000 days is assumed.

	c	p	α	K	branching ratio
Fitted to all sequences	0.016	1.06	0.74	0.016	0.60
Physics-based	0.00069	1.00	1.07	0.0028	0.41

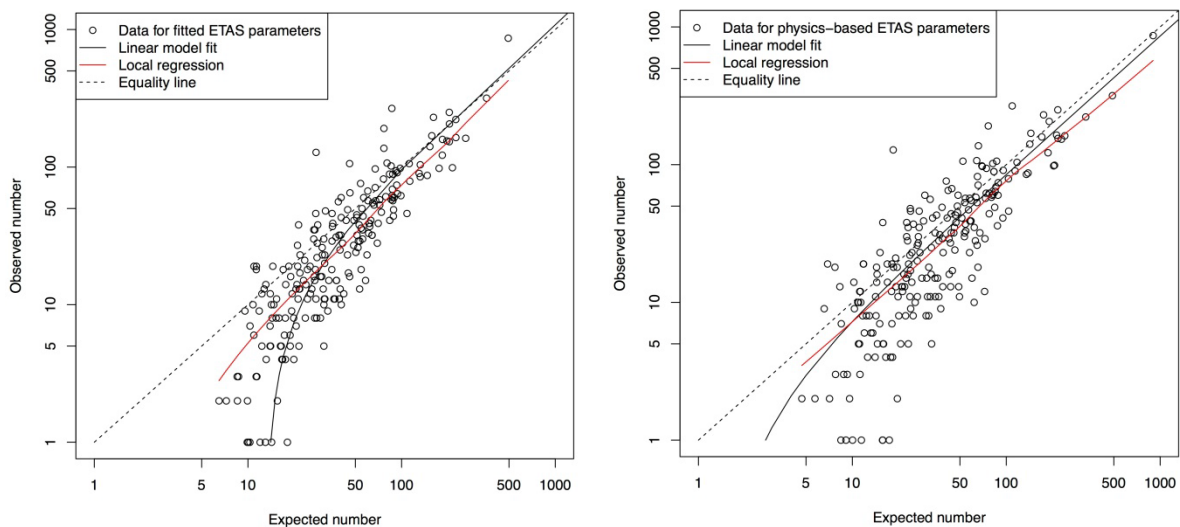


Figure 3.2 The observed versus expected number of forecasted aftershocks in time interval 1-365 days after the mainshock for two sets of ETAS model parameters; the first was fitted to all sequences, the second was derived from physics-based models.

The first difference compared to the New Zealand data is that the parameters were only fitted to the aftershock sequences and not to the complete catalogue including the overall background seismicity. Thus there is no bias from the non clusters. Due to the long tail of the distribution of the number of cascading aftershocks in the ETAS model, mostly through the power law decay in time, the median number of expected aftershocks can be significantly smaller than the mean. In Figure 3.3 we show for both sets of universal ETAS parameters how many clusters have a higher proportion of observed aftershocks than simulated. A value of 0.5 on the x-axis means that 50% of the 1,000 simulated aftershock sequences had more aftershocks than observed. If the universal ETAS parameters fitted all sequences well, then the graph would track the equality line. We tested the simulations by randomly drawing 1 out of the 1000 simulations and plotting them in a similar graph, and indeed the data were uniformly distributed and followed the equality line. Figure 3.3 indicated that about 30% of the simulations with physics-based ETAS parameters underfit the data, i.e. there are more observations than expected and the data are above the equality line. There is no systematic underfitting for the simulations with the fitted ETAS parameters all data are below the equality line. The results confirm what we already observed from the data in the literature: Universal ETAS parameters do fit some but not all the sequences well.

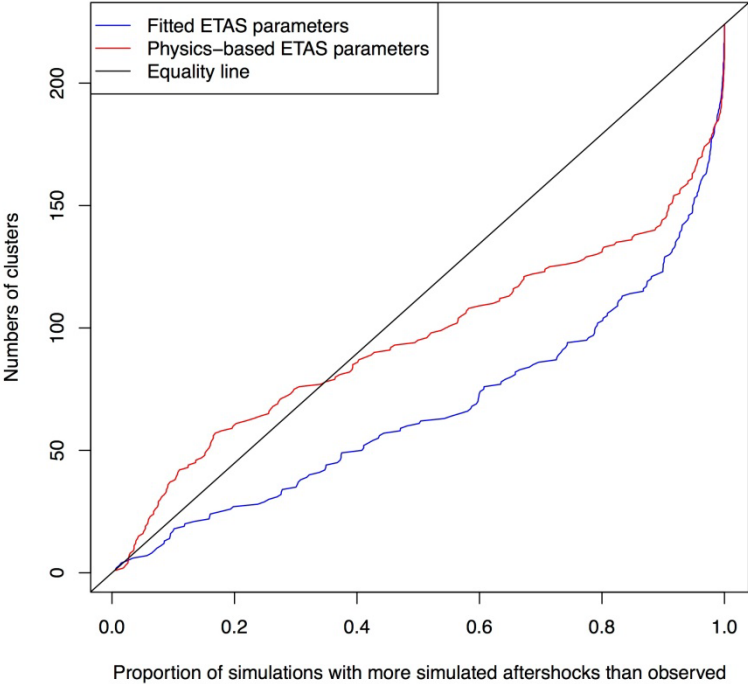


Figure 3.3 The number of clusters for 224 global sequences which have more simulated aftershocks than observed.

4.0 THE EFFECTIVE FORECASTING PERIOD T_F

We define the effective forecasting period T_F as the time following a mainshock, in which a time-varying earthquake clustering model provides a better estimate of future seismicity than a time-invariant (Poisson) estimate. In the case of the ETAS model any information on past earthquakes theoretically improves the forecasts at all later times if the ETAS parameters are known and the ETAS model was a perfect description of the seismicity. However, even if the ETAS model was a perfect description of real seismicity, the uncertainties in parameter estimation will limit the forecasting ability (Harte, 2013; Rhoades, 2013). These uncertainties may result in branching ratios larger than one and thus lead to estimates of seismicity escalating with time. Therefore a simple Poisson model might be a better estimator of future seismicity than an ETAS forecast from uncertain parameters.

The effective forecasting period T_F depends on several factors, including (1) the number and quality of data available; (2) the quality of the model, i.e. how well the model describes the observed seismicity; (3) the magnitude difference between mainshock and cut-off magnitude. To estimate an upper bound of T_F and to analyse the dependency on mainshock magnitude and the data available for parameter estimation, we conducted a numerical experiment. In our experiment we estimated the parameters of input earthquake sequences conforming to a known model from limited data sets; we then used the estimated parameters to forecast aftershock rates following large earthquakes; we measured the information gain of those forecasts against target earthquake sequences conforming to the known model. This experiment represents a best-case scenario where we know the correct model, and where an earthquake catalogue is available without any completeness problems or magnitude errors. Section 6 in the Appendix provides the details of the experiment and its results. Very high information gain is only observed in the first few hours after a mainshock. After approximately 100 days for $M = 6$ and 1000 days for $M = 7$, the mean information gains are close to zero or even negative, indicating that, on average, the forecast of the Poisson model becomes equal to or better than that of the modified ETAS model for times afterwards.

The quality of the ETAS forecasts clearly depends on the quality of the parameter estimates for the input sequences, as can be seen by the large spread between the different lines in Figure 7 in the Appendix. An increased input data set of $N = 500$ instead of 100 earthquakes preceding the mainshock leads to some improvement, but still the parameter uncertainties lead to strongly variable information gains.

5.0 CONCLUSIONS AND OUTLOOK

We investigated three different time scales of aftershock activity: (1) the triggering time T , which is the duration of the physical triggering process of a single event; (2) the apparent aftershock duration T_a which is the time period in which aftershocks dominate the seismicity; and (3) the effective forecasting period T_f within which earthquake rate estimates are significantly improved by time-dependent seismicity models after a large earthquake.

A finite value of T is expected from a physical point of view, but ignored in standard ETAS model applications so far. During this project we introduced and estimated for the first time finite T -values in the modified ETAS model. Although estimates of T were only weakly constrained and potentially subject to biases due to limited catalogue length and cluster selection, our comparative analysis of synthetic sequences gave some robust results: we found that T has an impact on the estimates of the other ETAS-parameters. We also found that the apparent mismatch between ETAS inverted p -values of the Omori-Utsu law and predictions of the rate-and-state friction model (Dieterich, 1994) was reduced when the ETAS inversion allowed for finite values of T . Furthermore, the predicted inverse proportionality between T and the background rate is in agreement with the observed trend in the estimated values of T for empirical earthquake sequences. The duration of the triggering process can be much longer than the apparent aftershock duration T_a .

We estimated the apparent aftershock duration T_a from the observed total aftershock rate and the background rate for all sequences with at least 50 earthquakes for three earthquake catalogues. There were large uncertainties in the parameter estimates, however, only few sequences lasted longer than 10 years. This is contrary to the common understanding that aftershocks can continue for decades. This is also not consistent with the aftershock models currently used in New Zealand, which model aftershocks continuing for thousands of years.

Very recently Mignan (2015) published a review paper on aftershock models. He concluded that aftershock decay was better modelled by a stretched exponential than by a power law like the Omori-Utsu law despite the prevalence of the Omori-Utsu law in aftershock models. The stretched exponential is consistent with a relaxation process as observed in other natural phenomena. It would not be difficult to replace the Omori-Utsu law within either the STEP or the ETAS model with a stretched exponential and test Mignan's hypothesis for New Zealand. However, this is beyond the scope of this project.

In this project, we demonstrated by means of simulations of the modified ETAS model that estimates of the apparent aftershock duration T_a are strongly dependent on the mainshock magnitude and the background level. Although the T_a estimates cannot be used to analyse the underlying physical process, they can serve as an estimate of the effective forecasting period T_f . We set up a numerical experiment to estimate T_f from simulated data. We found that after approximately 100 days for $M = 6$ and 1000 days for $M = 7$, the mean information gains are close to zero or even negative, indicating that, on average, the forecast of the Poisson model becomes equal to or better than that of the modified ETAS model for times afterwards. Given the short duration of the effective forecasting period and the short apparent durations of sequences T_a , we did not pursue our original goal to estimate the probability that the 1968 Inangahua earthquake was an aftershock of the 1929 Murchison earthquake.

Our findings confirm the conclusions from recent retrospective tests of the Canterbury earthquake model, to separate time-varying earthquake models into aftershock models and EEPAS models in future hybrid earthquake forecasts.

Our forecast experiment with universal ETAS parameters confirmed earlier work that universal ETAS parameters do not fit all sequences well. However, estimating parameters for an on-going sequence has too many uncertainties and does not lead to stable results. We did not investigate what universal set of parameters might be best.

Recent experience with the Wanaka earthquake showed that regular updating of the forecast with the seismic history provides reasonable forecasts because the ETAS model quickly adapts to the seismic history.

In summary, our project on “Testing aftershock models on time-scale of decades” answered the three questions we had raised in the proposal. We found that many aftershock sequences cannot be detected above the background seismicity for more than 1 year, and only few sequences last longer than 10 years. A universal set of ETAS parameters does not fit all earthquake sequences well but fitting the parameters to individual sequences introduces too many uncertainties. Finally, the effective forecasting time of the ETAS model is only in the order of 100 and 1000 days for mainshocks of M6 and M7, respectively.

6.0 ACKNOWLEDGEMENTS

This research was funded by the Earthquake Commission under grant number 14/TV682. This report has been internally reviewed by David Burbidge and Chris Van Houtte.

7.0 REFERENCES

- Christophersen, A., Rhoades, D.A., Hainzl, S., Smith, E.G.C., Gerstenberger, M.C. 2013. The Canterbury sequence in the context of global earthquake statistics. GNS Science Consultancy Report (2013/196), 28pp.
- Dieterich, J., 1994. A constitutive law for rate of earthquake production and its application to earthquake clustering. *J. Geophys. Res.* 99, 2601-2618.
- Dieterich, J., Cayol, V., Okubo, P., 2000. The use of earthquake rate changes as a stress meter at Kilauea volcano. *Nature* 408, 457-460.
- Evison, F.F., Rhoades, D.A., 2004. Demarcation and scaling of long-term seismogenesis. *Pageoph* 161, 21-45.
- Gerstenberger, M., McVerry, G., Rhoades, D., Stirling, M., 2014. Seismic Hazard Modeling for the Recovery of Christchurch. *Earthquake Spectra* 30, 17-29.
- Gerstenberger, M., Wiemer, S., Jones, L., 2004. Real-time Forecasts of Tomorrow's Earthquakes in California: a New Mapping Tool. United States Geological Survey Open-File Report, 2004-1390.
- Gerstenberger, M.C., Wiemer, S., Jones, L.M., Reasenber, P.A., 2005. Real-time forecasts of tomorrow's earthquakes in California. *Nature* 435, 328-331.
- Hainzl, S., 2013. Comment on 'Self-similar earthquake triggering, Båth's law, and foreshock/aftershock magnitudes: Simulations, theory, and results for Southern California' by P. M. Shearer. *J. Geophys. Res.* 118, 1188-1191.
- Hainzl, S., Christophersen, A., Enescu, B., 2008. Impact of earthquake rupture extensions on parameter estimations of point-process models. *Bull. Seism. Soc. Am.* 98, 2066-2072.
- Hainzl, S., Zakharova, O., Marsan, D., 2013. Impact of Aseismic Transients on the Estimation of Aftershock Productivity Parameters. *Bull. Seismol. Soc. Am.* 103, 1723-1732.
- Harte, D.S., 2013. Bias in fitting the ETAS model: a case study based on New Zealand seismicity. *Geophys. J. Int.* 192, 390-412.
- Helmstetter, A., Shaw, B.E., 2006. Relation between stress heterogeneity and aftershock rate in the rate-and-state model. *Journal of Geophysical Research: Solid Earth* 111, B07304, doi:10.1029/2005JB004077.
- Ogata, Y., 1988. Statistical models for earthquake occurrences and residual analysis for point processes. *Journal of American Statistical Association* 83, 9-27.
- Omori, F., 1894. On aftershocks. Report of Imperial Earthquake Investigation Committee 2, 103-109.
- Pollock, D., 2007. Aspects of short-term and long-term seismic hazard assessment in New Zealand, Department of Earth Sciences, Master thesis, ETH Zurich.
- Rhoades, D.A., 2013. Mixture models for improved earthquake forecasting with short-to-medium time horizons. *Bull. Seismol. Soc. Am.* 103, 2203-2215.

- Rhoades, D.A., Evison, F.F., 2004. Long-range earthquake forecasting with every earthquake a precursor according to scale. *Pageoph* 161, 47-72.
- Rhoades, D.A., Evison, F.F., 2005. Test of the EEPAS Forecasting Model on the Japan Earthquake Catalogue. *Pageoph* 162, 1271-1290.
- Rhoades, D.A., Gerstenberger, M.C., Christophersen, A., Liukis, M., 2013. Utilising short-term and medium-term forecasting models for earthquake hazard estimation in the wake of the Canterbury earthquakes. GNS Science Consultancy Report.
- Rhoades, D.A., Liukis, M., Christophersen, A., Gerstenberger, M.C., 2016. Retrospective tests of hybrid operational earthquake forecasting models for Canterbury. *Geophys. J. Int.* 204, 440-456.
- Utsu, T., Ogata, Y., Matsu'ura, R.S., 1995. The centenary of the Omori formula for a decay law of aftershock activity. *Journal of the Physics of the Earth* 43, 1-33.

APPENDIX

A1.0 STATISTICAL ESTIMATION OF THE DURATION OF AFTERSHOCK SEQUENCES

Statistical estimation of the duration of aftershock sequences

S. Hainzl¹, A. Christophersen², D. Rhoades², D. Harte²

¹ GFZ German Research Centre for Geosciences, Potsdam, Germany (hainzl@gfz-potsdam.de)

² GNS Science, Lower Hutt, New Zealand

28 December 2015

SUMMARY

It is well-known that large earthquakes generally trigger aftershock sequences. However, the duration of those sequences is unclear due to the gradual power-law decay with time. The triggering time is assumed to be infinite in the epidemic type aftershock sequence (ETAS) model, a widely-used statistical model to describe clustering phenomena in observed earthquake catalogues. This assumption leads to the constraint that the power-law exponent p of the Omori-Utsu decay has to be larger than one to avoid supercritical conditions with accelerating seismic activity on long time scales. In contrast, seismicity models based on rate- and state-dependent friction observed in laboratory experiments predict $p \leq 1$ and a finite triggering time scaling inversely to the tectonic stressing rate. To investigate this conflict, we analyse an ETAS model with finite triggering times, which allow smaller values of p . We use synthetic earthquake sequences to show that the assumption of infinite triggering times can lead to a significant bias in the maximum likelihood estimates of the ETAS parameters. Furthermore, it is shown that the triggering time can be reasonably estimated using real earthquake catalogue data, although the uncertainties are large. The analysis of real earthquake catalogues indicates mainly finite triggering times in the order of 100 days to 10 years with a weak negative correlation to the background rate, in agreement with expectations of the rate- and state-friction model. The triggering time is not the same as the apparent duration, which is the time period in which aftershocks dominate the seismicity. The apparent duration is shown to be strongly dependent on the mainshock magnitude and the level of background activity. It can be much shorter than the triggering time. Finally, we perform forward simulations to estimate the effective forecasting period, which is the time period following a mainshock, in which ETAS simulations can improve rate estimates after the occurrence of a mainshock. We find that this effective forecasting period is only in the order of 100 days for moderate mainshocks and in the order of a few years for large events, even if the underlying triggering process lasts much longer.

Key words: Statistical Seismology, Earthquake interaction, forecasting and prediction.

1 INTRODUCTION

Aftershock triggering following large earthquakes is ubiquitous in seismicity dynamics. Most aftershocks occur close to the mainshock rupture with an occurrence rate R which can be well described by the Omori-Utsu law

$$R(t) = K_0(t + c)^{-p} \quad (1)$$

where t indicates the elapsed time since the mainshock; see Utsu et al. (1995) for a review. The parameter K_0 is known to depend on the mainshock magnitude M , while p is typically in the range 0.8–1.2 and independent of M (Utsu et al. 1995). The time-offset parameter c is generally much less than 1 day, and is usually related to reduced detection ability of the operating seismic network immediately after large events (Kagan 2004).

While the Omori-Utsu decay generally provides a good fit to the data at short times, its applicability to longer times is questionable (Harte 2013). This raises questions about the duration of the sequence. Sometimes the aftershock duration is considered to be the time period in which aftershock activity dominates the overall seismicity. However, this is only an apparent duration, which depends on the aftershock productivity and the background level. It is a lower limit of the true duration of the underlying physical triggering process, which might be minor but still on-going. The estimation of the latter is also hampered by the frequent occurrence of large aftershocks, which trigger their own local aftershock sequence. To account for this secondary triggering, the Epidemic Type Aftershock Sequence (ETAS) model has

been developed. It is a stochastic point process model that builds on the Omori-Utsu law and also takes stationary background seismicity and secondary aftershocks into account (Ogata 1988; Helmstetter & Sornette 2002). In the ETAS model, each earthquake has a magnitude-dependent ability to trigger aftershocks with an intensity proportional to $K 10^{\alpha(M_i - M_{\min})}$, where α and K are constants and M_{\min} is the lower magnitude cut-off of the earthquakes under consideration. In this model, the total rate at time t is the sum of background seismicity and ongoing aftershocks triggered by all past events. The total occurrence rate of earthquakes is given by

$$R(t) = \mu + \sum_{i:t_i < t} \frac{K 10^{\alpha(M_i - M_{\min})}}{(t - t_i + c)^p} \quad (2)$$

with μ being the background rate. A necessary condition for stability of forward simulations is that the aftershock sequences decay sufficiently fast, namely with $p > 1$. Otherwise the total number of aftershocks would become infinite for long times and the total seismicity would escalate with time (Zhuang et al. 2013; Harte 2013).

However, physics-based aftershock models predict $p \leq 1$ for direct aftershocks, which would lead to unstable solutions of the ETAS model. In response to static stress changes, aftershock triggering can be explained in terms of stress corrosion or rate-and-state dependent frictional nucleation. Experimental studies show that the transition rate to rupture can be described by an exponential function (Scholz 2002) or a power-law function of the overload value (Atkinson 1984). Assuming that the pre-stress values are uniformly distributed, the resultant earthquake rate corresponds to the Omori-Utsu law with $p = 1$ in the case of an exponential transition function with an exponential roll-off at larger times (Narteau et al. 2002). The framework of rate-and-state friction (Dieterich 1994; Dieterich et al. 2000), which takes into consideration the rate- and slip-dependence of frictional strength and time-dependent restrengthening observed in laboratory experiments, yields similar results. In this frictional regime, the rate of triggered aftershocks in response to a stress jump ΔCFS at time $t = 0$ evolves according to

$$R(t) = \frac{\mu}{1 + \left(e^{-\frac{\Delta\text{CFS}}{A\sigma}} - 1 \right) e^{-\frac{t}{t_r}}} - \mu \quad (3)$$

with the frictional resistance $A\sigma$ and the aftershock relaxation time t_r which is inversely proportional to the tectonic stressing rate $\dot{\tau}$, i.e. $t_r = A\sigma/\dot{\tau}$. The response is equal to the Omori-Utsu decay with $p = 1$, $K = \mu t_r$ and $c = t_r / (\exp(\Delta\text{CFS}/A\sigma) - 1)$ with an exponential roll-off at time t_r (Cocco et al. 2010). For realistic cases with space-dependent coseismic stress changes, the model leads to an overall seismicity decay with an exponent even smaller than 1 (Helmstetter and Shaw 2006).

The $p > 1$ -values that are usually estimated by means of the ETAS model seem to contradict these physical models. However, ETAS applications are so far based on the assumption of infinite triggering times, which is inconsistent with $p \leq 1$ on long time scales, as mentioned above. Previous analysis already indicated that finite aftershock durations can significantly affect the interevent-time distribution (Shcherbakov et al. 2005). Here we will show that this inconsistent model assumption can also lead to biased results in ETAS estimation and that applications of the ETAS model with temporally limited aftershock triggering leads to p -value estimates that are more consistent with the rate-and-state friction model. While some previous analysis was performed rather qualitatively, e.g. (Stein and Liu 2009), we estimate for the first time the duration of the triggering process by means of the modified ETAS model fitted to observed catalogue data. In particular, we want to distinguish between three different time scales of an aftershock process:

- T : the duration of the physical triggering process of a single event, hereinafter called the triggering time;
- T_a : the apparent duration in which aftershocks dominate the total seismicity; and
- T_f : the effective forecasting period, which is the time period in which a time-dependent model of aftershock occurrence improves the earthquake rate calculations.

2 DATA

To study the role of finite triggering time T , we investigate simulations of the ETAS model as well as observed data from two regional catalogues and one global catalogue. By utilising synthetic sequences, we can evaluate potential biases of ETAS inversions, because we know the true underlying parameter values. This helps us to interpret results obtained from the observed data.

2.1 ETAS simulations

We analyse Monte-Carlo simulations of the ETAS model, where we ignore the spatial component of the triggering process for computational efficiency. In these simulations, a doubly-truncated Gutenberg-Richter law is assumed for the magnitude distribution, with minimum and maximum magnitudes of $M_0 = 2$ and $M_{\max} = 7$ and a b -value of 1. The minimum value M_0 is set to be smaller than the minimum magnitude M_{\min} of the later analysis to consider the realistic effect that earthquakes with magnitudes less than the observational cut-off magnitude (M_{\min}) have triggered some of the earthquakes above this threshold. We assume a constant background rate of 10^{a-bM_0} [1/yr] of $M \geq M_0$ events; where the a -value defines the activity level. The ETAS parameters are set to the values $p = 1.0$, $c = 0.01$ days, and $\alpha = b = 1.0$, while we test the effect of using different values of the triggering time T . Finally, for given parameters c, p, α , and T , we

determine K indirectly by setting the branching ratio n to a reasonable value. The branching ratio is the average number of events directly triggered by an individual earthquake. It can be calculated by (Helmstetter et al. 2005)

$$n = \int_{M_0}^{M_{\max}} \text{pdf}(M) K 10^{\alpha(M-M_0)} \int_0^T (t+c)^{-p} dt dM, \quad (4)$$

where $\text{pdf}(M)$ is the probability density function of the earthquake magnitudes, i.e. the doubly-truncated Gutenberg-Richter distribution. Depending on the value of the branching ratio, it is possible to separate significantly different cases of model behaviour: a branching ratio of $n > 1$ leads to escalating seismic sequences; $0 < n < 1$ describes a stationary regime; while $n = 0$ implies that all events are independent and thus represents a Poisson process. Observational evidence indicates a branching ratio in the range 0.5–1.0 (Sornette and Werner 2005). In our simulations, we assume $n = 0.8$ to set the K -value. Finally, the a -value of the background activity is set to 4, if not mentioned otherwise.

With these ETAS parameters we simulated sequences over 40 years. We removed the first 10 years to avoid transient effects and cut all events below magnitude $M_{\min} = 3.0$. Thus the synthetic catalogues finally analysed consist of $M \geq 3$ events spanning a time period of 30 years, similar to the periods of the observational catalogues analysed in this paper.

2.2 Observational Data

The analysed empirical mainshock-aftershock sequences are selected from the following three catalogues:

California catalogue (CA):

We use the relocated high-resolution Southern California catalogue containing earthquakes from 1981 to 2011 in the region extending from Baja California in the south to Coalinga and Owens Valley in the north (Hauksson et al. 2012). This area is roughly rectangular ranging from 30° to 37.5° latitude and from -113° to -122° longitude. We use a cutoff magnitude of $M_{\min} = 3.0$ which ensures complete recordings leading to 12,105 earthquakes above this threshold.

New Zealand catalogue (NZ):

We use the GeoNet catalogue of New Zealand earthquakes which, until the end of 2011, was processed by the CalTech-USGS seismic processor (CUSP) system (Lee and Stewart 1989). We selected earthquakes inside the testing region of the Collaboratory for the Study of Earthquake Predictability (CSEP). This region includes the main islands of New Zealand and extends about 50 km offshore with a depth cut-off of 40km (Gerstenberger and Rhoades 2010). Considering changes in the magnitude of completeness over time, we extract two versions: (1) $M_{\min} = 4.0$ from 1964 to 2011 (7136 events); and (2) $M_{\min} = 3.5$ from 1987 to 2011 (18,969 events).

Global catalogue (global):

We analyse the global USGS PDE catalogue in the time period between 1973 and 2011. To ensure completeness, we use the cut-off magnitude of $M_{\min} = 5.0$ and select only shallow events with a depth less than 50 km. This selection yields a catalogue of 43,521 events.

2.2.1 Cluster selection

No unique procedure exists for separating seismic events into mainshocks (independent earthquakes) and aftershocks (dependent earthquakes). Several alternative cluster selection procedures have been introduced in the past (see review by van Stiphout et al. (2012)). In our work, we follow the window-based procedure of Tahir et al. (2012) for cluster determination. An earthquake with magnitude M is defined as a mainshock if it is the largest earthquake within the time period $\pm \tilde{T}$ and distance range $D(M)$. The spatial window is set to be a multiple of the rupture length, i.e. $D(M) = \tilde{D} L(M)$, where $L(M) = 10^{-2.44+0.59M}$ [km] is the average rupture length of an earthquake with magnitude M (Wells and Coppersmith 1994) and \tilde{D} is a selectable constant. The parameters are chosen in accordance with general observations of aftershock occurrences. It is known that the majority of aftershocks occur very close to the mainshock rupture. Nevertheless, remotely triggered aftershocks can also occur far away and these events will be missed for small values of \tilde{D} . As a compromise, we choose $\tilde{D} = 3$ but test the robustness of our results also for different values (see electronic supplemental material). Furthermore, we choose $\tilde{T} = 1$ year because the majority of aftershocks, namely 82% (70%), are expected to occur within one year in the case of an Omori-Utsu decay with $p = 1$, $c = 0.01$ days, and a total aftershock duration of 10 (100) years. However, as described below, our procedure also accounts for the effect of earthquakes outside the selection radius and time window and for effects of background earthquakes. Consequently, our results are less dependent on the specific parameter choice than if we used hard limits and gave no consideration to background seismicity.

After the identification of a mainshock with magnitude M , we fit the ETAS model to earthquakes occurring in the circular area with radius $D(M)$ around the mainshock epicentre in the time interval from 1 year before the mainshock until the end of the catalogue. Within this period we exclude time intervals of incompleteness in the catalogue known to occur after mainshocks (Kagan 2004). For that we use the estimated incompleteness function for California, $M_c(M, \Delta t) = M - 4.5 - 0.75 \log_{10}(\Delta t)$, where Δt is the time (in days) after an earthquake with magnitude M (Helmstetter et al. 2006). Earthquakes in time periods with $M_c > M_{\min}$ are not considered as target events, but still contribute to the predicted ETAS rate in later time periods. This approach has been shown to prevent biased parameter estimations

of the ETAS model (Hainzl et al. 2013). Similarly, earthquakes outside the target region are expected to influence the seismicity rate within the test region. To calculate the spatial impact factor of each earthquake, we consider the empirical probability density distribution recently derived for California seismicity consisting of three different regimes with transitions at the scale of the rupture length and the thickness of the crust (Moradpour et al. 2014). It is described as a function of the epicentral distance r by the functional form

$$P(M, r) = \begin{cases} c_1 \frac{q r^\gamma}{r_M^{\gamma+1} \left(\frac{r^{\gamma+1}}{r_M^{\gamma+1}} + 1 \right)^{1+\frac{q}{\gamma+1}}} & \text{if } r < R_c, \\ c_2 \frac{d r^\gamma}{r_M^{\gamma+1} \left(\frac{r^{\gamma+1}}{r_M^{\gamma+1}} + 1 \right)^{1+\frac{d}{\gamma+1}}} & \text{if } r > R_c, \end{cases} \quad (5)$$

with normalizing constants c_1 and c_2 , parameters $\gamma = 0.6, q = 0.35, d = 1.2$, a cross-over distance $R_c = 10$ km, and r_M related to the earthquake magnitude M according to $r_M = 5 \cdot 10^{-3+0.44M}$ km (Moradpour et al. 2014). Note that this empirical distribution is found to be in agreement with static stress triggering (Hainzl et al. 2014). Although the spatial distribution function has so far been fitted only to California data, Hainzl et al. (2014) showed in their electronic material that the distribution is not strongly dependent on the focal mechanism. Thus we use Eq.(5) with the same parameters for all empirical data. The fraction of aftershocks of a mainshock located at \vec{x}_i expected to occur inside the analysed circular area A is calculated by the integral $w_i = \int_A P(M, |\vec{x} - \vec{x}_i|) d\vec{x}$ and enters in the modified rate function as

$$R(t) = \mu + \sum_{i:0 < t-t_i < T} \frac{w_i K 10^{\alpha(M_i - M_{\min})}}{(t - t_i + c)^p}, \quad (6)$$

where the index i ranges over all earthquakes in the catalogue with magnitudes $\geq M_{\min}$, including events outside A , but only over events that occur no longer than T before t (i.e. the Omori tail is truncated to a maximum length of T). We will refer to this as the *modified* ETAS model. When the summation is taken over all events before t (i.e. no truncation), we will refer to this as the *standard* ETAS model. To ensure some statistical significance, we restrict our analysis to mainshocks with magnitude $M \geq M_{\min} + 1.5$ for which $N \geq 50$ events occurred within distance $D(M)$ in the complete time periods between 1 year prior to the mainshock and the end of the catalogue.

2.3 Parameter estimation

For N observed earthquakes occurring within an area A in one of the N_k sub-periods with complete recordings (see above), we estimate ETAS parameters (μ, c, p, K, α) by maximizing the Log-Likelihood function $\mathcal{L}\mathcal{L}$

$$\mathcal{L}\mathcal{L} = \sum_{j=1}^N \ln(R(t_j)) - \sum_{k=1}^{N_k} \int_{t_s^{(k)}}^{t_e^{(k)}} R(t) dt \quad (7)$$

where $t_s^{(k)}$ and $t_e^{(k)}$ refer to the start and end times of the k th complete subinterval. Note that incompleteness periods defined by the empirical function for California are also excluded in the case of synthetic simulations to ensure comparability. In both cases, we consider the incomplete periods after all $M \geq M_{\min} + 2$ events. In Eq.(7), R is given by Eq.(6), where w_i -values are equal to the calculated spatial weights in the case of real catalogues and set to 1 in the case of synthetic simulations. Our parameter estimates are calculated by the following steps: (i) For given T , all other parameters are optimized by the Davidon-Fletcher-Powell optimization algorithm yielding the maximum Log-Likelihood value $\mathcal{L}\mathcal{L}_{\max}(T)$ (Press et al. 1992). (ii) A grid-search for T between 10 days and the total length of the catalogue is conducted to find the overall maximum $\mathcal{L}\mathcal{L}_{\max} = \max_T \{\mathcal{L}\mathcal{L}_{\max}(T)\}$ and the corresponding parameter values.

3 RESULTS - PARAMETER BIAS

We analyse the bias in parameter estimates induced by having a truncated Omori tail but estimating the parameters using the standard ETAS model which assumes infinite T , see definitions after Eq. (6). First, we investigate simulations of the modified ETAS model for which we know the true underlying triggering parameters. To study the dependence of the results on the decay rate of the Omori-Utsu relation, we use simulations with p varying between 0.8 and 1.2 in steps of 0.1 and T taking values of 100 or 1600 days. For each parameter set, we perform 100 synthetic simulations for which we then estimate the standard ETAS parameters using the maximum likelihood method for the catalogue length of 30 years, assuming the triggering time to be infinite ($T = \infty$).

Figure 1 shows the resulting distributions of estimated parameters as box plots. The results show that the estimation of the α -parameter is almost unbiased, while all other parameters are significantly biased for $T = 100$ days, $T = 1600$ days, or both. In particular, parameters c and p , whose estimates are known to be positively correlated (Holschneider et al. 2012; Harte 2015), are both strongly overestimated in the case of $T = 100$ days. This bias is strong for small values of p and decreases as p increases. However, both parameters show almost no bias in the case of $T = 1600$ days. The same holds for the estimation of K which is significantly overestimated for $T = 100$ days, but almost unbiased for $T = 1600$ days. In contrast, the estimates of μ are biased for both $T = 100$ and $T = 1600$ days. The underestimation of μ can

be understood from the fact that background events occurring after the end of an aftershock sequence ($t > T$) might be wrongly associated with this sequence, because $T = \infty$ is assumed in the inversion. Larger values of p correspond to faster aftershock decay making such wrong associations less likely and thus reducing the bias in the estimates of μ . It should be noted that some bias of the parameter estimates would also be present in the case of simulations with $T = \infty$, because of finite size effects, particularly the missing $M < M_{\min}$ events (Harte 2015).

Our observation that maximum likelihood can overestimate the parameter p when assuming $T = \infty$ can help to explain the discussed discrepancy between physics-based seismicity models forecasting $p \leq 1$ and the standard ETAS model finding values above 1. For example, in the case of $T = 100$ days, the estimates of p are in the range 1.0–1.2 for true input values ranging between 0.8 and 1.0.

Now we perform a similar analysis for the empirical sequences selected from the observed catalogues. We again estimate the standard ETAS parameters by the maximum likelihood method assuming $T = \infty$. However, in contrast to the synthetic sequences, we cannot directly compare with true parameter values. Instead we compare the estimates with those for the triggering time T that maximizes the log-likelihood (Eq. 7). The distribution of the maximum likelihood estimates of T are shown in Fig. 2. The results show that most estimated values of T are shorter than 1000 days and thus significantly shorter than the catalogue lengths, without any clear correlation with the mainshock magnitudes. The modified ETAS parameters corresponding to these estimated T -values are compared in the scatter plots of Fig. 3 with those values estimated for $T = \infty$. We can recognize the same patterns as for the synthetic sequences. The parameters with $T = \infty$ are systematically overestimated compared to those for estimated T in the case of c and p , underestimated in the case of the background rate μ , and almost unbiased in the case of α . In particular, the median value of p is 1.04 (1.01) for estimated T , and 1.10 (1.07) for $T = \infty$, in the case of a cluster selection parameter $\tilde{D}=3.0$ (5.0). The new estimates are close to the value indicated by the physics-based models (Dieterich 1994; Narteau et al. 2002).

4 RESULTS - TRIGGERING TIME T

In the previous section, we presented modified ETAS-parameter estimates based on the maximum likelihood fit of the triggering time T . For synthetic earthquake catalogues, we now verify that the fitted value is a reasonable estimate of the true underlying T -value, although subject to large uncertainty. For that purpose, we adapt our simulations and the estimation procedures to be as consistent as possible with those for the observational data in order to test the resolution power in the case of similarly limited data. We analyse simulations of 30 years (see Sec. 2.1) and select only mainshocks with $M \geq M_{\min} + 1.5$ occurring during this period with $N \geq 50$ earthquakes for the \mathcal{LL} -estimation. We assume different levels of the background rate by changing the Gutenberg-Richter a -value systematically from 1.6 to 5.0 with step size of 0.2, where 100 mainshocks are selected for each background level.

For each of these sequences, we determine the triggering times T corresponding to the maximum \mathcal{LL} (see Eq. 7) and to $\Delta\mathcal{LL} = 0.5$ and 2, which are related to one and two standard deviations, respectively, in the case that the likelihood function can be approximated by a normal distribution. Figure 4 shows the estimated values of T as a function of the estimated background rates for sequences simulated with $T = 365, 1000, \text{ and } 10,000$ days. The points refer to the maximum likelihood estimates of T , while the background colors refer to the stacked probability density functions (approximated by a lognormal distribution) of the estimates in bins of the rate values. The uncertainties are often very large. However, our results indicate that shorter triggering times up to $T = 1000$ days can be rather well recovered, while the estimates are almost unconstrained for larger T -values.

We now calculate the corresponding results for the observational data. As shown in Fig. 2a, most estimated values of T are shorter than 1000 days for the selected clusters. Individually, the estimated small T -value might result only from the large intrinsic uncertainties as seen e.g. in Fig. 4. However the difference of the distribution of estimated T -values to that in Fig. 4c indicates that the empirical data are not in agreement with infinite triggering times. Figure 5a shows the results as a function of the estimated background rates μ , where the background grey scale refers to the stacked probability functions of the estimates as in Fig. 4. The results are found to be significantly different from Fig. 4c indicating once more that at least some T -values are smaller than 10,000 days.

In order to compare the results of the different data sets with different M_{\min} and to account for the mainshock-dependent spatial area $A(M) = \pi D(M)^2$, we transformed the background estimate into an earthquake occurrence rate density of $M \geq 0$ events by multiplication with $10^{bM_{\min}}/A(M)$. The results corresponding to a fixed b -value of 1 are presented in Fig. 5b, while the results for individually estimated b -values are illustrated in Fig. S5 of the electronic supplement. The results show a tendency for T to be inversely proportional to the background rate density, $T \propto 1/\mu$, although the uncertainties of the individual estimates are generally large. In particular, weak inverse relations are found for the two regional data sets of California and New Zealand, while the results for the global data set show no clear trend. An inverse proportionality is in agreement with forecasts of the rate-and-state dependent frictional response of fault networks to mainshock-induced static stress changes. This model predicts an inverse relationship between the triggering time and the tectonic stressing rate (Dieterich 1994). Based on Kostrov's general results for the seismic deformation of rocks (Kostrov 1974), the background seismicity rate is expected to be proportional to tectonic stressing rate (Catalli et al. 2008; Hainzl et al. 2010). Thus an inverse relationship between T and μ is expected, corresponding to a decay with slope of -1 in a doubly logarithmic scale as indicated by the dashed line in Fig. 5b.

5 RESULTS - APPARENT AFTERSHOCK DURATION T_a

The triggering time T sometimes gets confused with the apparent aftershock duration T_a , in which aftershock activity is dominant. Here we define T_a as the time taken for the Omori-Utsu rate to decrease to a value that is equal to the background rate, i.e. $R(T_a) = \mu$, where $R(t)$ is defined by Eq. (1). It then follows that $T_a = (K_0/\mu)^{1/p} - c$. In this case, the total aftershock rate is considered, including secondary aftershock triggering. In contrast, the estimates of T apply to aftershocks directly triggered by each earthquake. T_a indicates the time scale in which aftershocks dominate the total seismicity and thus it is important for seismic hazard estimation. However, T_a is not necessarily related to the triggering time. In the ETAS model, the number of triggered aftershocks scales with the mainshock magnitude and thus T_a also scales with the mainshock magnitude. T_a also depends on the background level μ . To demonstrate this, we have performed simulations using the modified ETAS model with fixed $T = 1000$ days, variable background rates μ , and selected mainshocks of specific magnitudes. For each mainshock, we have estimated the parameters μ, K_0, c, p related to the model rate $R(t) = \mu + K_0(t + c)^{-p}$ within ± 1 year relative to the mainshock by means of maximum likelihood estimation. Note that these parameters take the effects of secondary and higher order aftershocks into account, in contrast to the results of the ETAS model application where parameters are related to aftershocks directly triggered by one mother event. The inverted parameters are then used to estimate T_a by the condition that $R(T_a) = 2\mu$, that is, the aftershock rate equals the background rate. The results are shown in Fig. 6a. It is obvious that this estimation is strongly dependent on the mainshock magnitude and inversely proportional to the background rate, while the triggering time is in all cases the same ($T=1000$ days). Thus T_a and T are quite different quantities.

We repeat the same estimation of T_a for the selected sequences from the empirical earthquake catalogues. The results presented in Fig. 6b show a similar time dependence of the T_a estimates on the background rates and mainshock magnitude (relative to the minimum magnitude of the catalog) as the results for the synthetic earthquake sequences.

Although T_a and T are almost independent quantities, T_a is related to how well the estimation of the triggering time T is constrained. The T -value estimation is better constrained for sequences with significant ongoing aftershock activity at time T , that is, in the case of large T_a . If T_a is estimated from first aftershocks, as done here, this means that T -estimations are expected to be well-constrained for $T_a \geq T$. As shown above, the T_a -values depend on the mainshock magnitude and the background rate. Thus T can be best estimated for large mainshocks and low background rates. This is seen in Fig. S6 of the electronic supplement, in which shorter confidence intervals reflect better estimation.

6 EFFECTIVE FORECASTING PERIOD T_f

The third important time scale of aftershock sequences is the effective forecasting period, which is the time scale on which a time varying estimate of the future seismicity rate is more informative than a time-invariant (Poisson) estimate following a mainshock. This time scale can be longer or shorter than the apparent aftershock duration T_a , but it will typically be much shorter than the duration T of the triggering process, because of uncertainties in specifying the model and in estimating its parameters. In the case of the ETAS model, any information on past events would theoretically improve forecasts at all later times if the ETAS parameters were known and the ETAS model were a perfect description of reality. However, even if the ETAS model is correct, the rather large uncertainties in the parameter estimates due to usually small sample sizes will limit the forecasting ability (Harte 2013; Rhoades 2013). In particular, these uncertainties often result in branching ratios larger than 1 which lead to unrealistic forecasts of seismicity escalating with time. Thus a simple Poisson model might become superior after some time. In the following, we define the effective forecasting period T_f by the condition that a Poisson model which is based on the average rate observed in the past will lead to similar or better estimates of the earthquake rate after time T_f .

T_f will depend on several factors, including (i) the number and quality of data available for parameter inversion, (ii) the correctness of the specified model, and (iii) the magnitude of the mainshock under consideration. To get some indication of the expected upper limit of T_f -values, and to investigate the effects on the number of data and the magnitude of the mainshock, we carry out a numerical experiment. In our experiment: the parameters of input earthquake sequences conforming to a known model are estimated from limited data sets; then the estimated parameters are used to forecast aftershock rates following large earthquakes; and the information gain of those forecasts is measured against target earthquake sequences conforming to the known model. This represents a best case scenario where we know the correct model, and where an earthquake catalogue is available without any completeness problems or magnitude errors.

For the purpose of our experiment, we use simulations of the modified ETAS model with Gutenberg-Richter distributed magnitudes in the range $[3 - 8]$ with $b = 1$, an a -value of 4.0 for the background seismicity, and $T = 10,000$ days, while all other parameters remain the same as before. Although each simulation provides an input catalogue of 10,000 days, only the $N = 100$ or 500 latest events are used as a learning set for parameter estimation, to account for realistic scenarios where complete recordings exist only in the most recent time period Δt . We estimate the ETAS parameters for each sequence. Then, using these estimated parameters, we estimate the future earthquake rate by generating 1000 forecast simulations and calculating the average forecast rate $\tilde{R}(t)$ for the first 10,000 days following a mainshock of magnitude M which occurs at the end of the input sequence. The information value of $\tilde{R}(t)$ is measured in comparison to a set of 100 simulated target sequences of future aftershock activity which are calculated with the true ETAS parameters. For each target aftershock sequence, we calculate the log-likelihood $\mathcal{LL}_{ETAS,i}$ -values of the modified ETAS model forecast $\tilde{R}(t)$ in time bins $[t_{i,1}, t_{i,2}]$. For comparison, in each case, we also calculate the $\mathcal{LL}_{Poisson,i}$ -value of the Poisson model forecast based on the rate estimation from the learning period, $N/\Delta t$. From these two log-likelihood values we determine the information gain $IG_i = (\mathcal{LL}_{ETAS,i} - \mathcal{LL}_{Poisson,i}) / (N_i + 1)$,

where N_i is the number of earthquakes observed in $[t_{i,1}, t_{i,2}]$. Positive IG-values indicate that the modified ETAS model forecast is an improvement on the Poisson model forecast.

Figure 7 shows the resulting IG-value averaged over the target aftershock sequences (solid lines) and the fraction of target sequences for which the $IG > 0$ (dashed lines) as function of time $\bar{t}_i = (t_{i,1} + t_{i,2})/2$. These two variables are plotted for 10 different input catalogues as functions of time after mainshocks with magnitudes of 6 and 7. As expected, the mean value of the information gain and the distribution of T_f both depend on the mainshock magnitude. The highest mean IG-value is about 2 in the case of $M = 6$ events and about 7 in the case of $M = 7$ mainshocks. However, these high values are only observed for the first few hours after the mainshock, because the information gains decay exponentially with time. After approximately 100 days for $M = 6$ and 1000 days for $M = 7$, the mean information gains are close to zero or even negative, indicating that, on average, the forecast of the Poisson model becomes equal to or better than that of the modified ETAS model for times afterwards. The quality of the ETAS forecasts clearly depends on the quality of the parameter estimates for the input sequences, as can be seen by the large spread between the different lines in Fig. 7. An increased input data set of $N = 500$ instead of 100 earthquakes preceding the mainshock leads to some improvement, but still the parameter uncertainties lead to strongly variable information gains. Finally, we compare these results with the estimates of the apparent aftershock duration T_a discussed in the previous section. T_a is the estimated time when the seismicity rate is twice the background rate, which would still indicate some forecast improvements at that time. The T_a estimates are calculated for the same background rate used for the IG estimates. The results are indicated by the vertical grey bar in Fig. 7 enclosing the 25% and 75% quantiles of the T_a estimates. It can be seen from the dashed lines and the vertical grey bars that T_f is highly variable, and that T_a overestimates T_f in many cases and underestimates it in others. Overall, T_a is close to the median of the T_f values. Note that T_f is expected to be even more variable, and likely shorter on average, for realistic input sequences with typical problems, such as missing events and magnitude errors, which will tend to increase the uncertainties of parameter estimates.

7 CONCLUSIONS

Aftershock activity involves three different time scales which are important for different purposes: (i) the triggering time T , which is the duration of the physical triggering process of a single event; (ii) the apparent aftershock duration T_a which is the time period in which aftershocks dominate the seismicity; and (iii) the effective forecasting period T_f within which earthquake rate estimates are significantly improved by time-dependent seismicity models after a large earthquake. A finite value of T is expected from a physical point of view, but ignored in standard ETAS model applications so far. Here, for the first time, we introduce and estimate finite T -values in the modified ETAS-model. Although T -estimations are only weakly constrained and potentially subject of biases due to limited catalogue length and cluster selection, our comparative analysis of synthetic sequences show some robust results: At first, we find that T has an impact on the estimates of the other ETAS-parameters. We find that the apparent mismatch between ETAS-inverted p -values of the Omori-Utsu law and predictions of the rate-and-state friction model (Dieterich 1994) is reduced when the ETAS inversion allows for finite values of T . Furthermore, the predicted inverse proportionality between T and the background rate is in agreement with the observed trend in the estimated values of T for empirical earthquake sequences. The duration of the triggering process can be much longer than T_a which is estimated from the observed total aftershock rate and the background rate. By means of simulations of the modified ETAS model, we have demonstrated that estimates of T_a are strongly dependent on the mainshock magnitude and the background level. Although the T_a estimates cannot be used to analyse the underlying physical process, they can serve as an estimate of the effective forecasting period T_f . However, T_f is highly variable and often smaller than T_a because of the uncertainties in the parameter estimates.

ACKNOWLEDGMENTS

We are grateful to the Editor Yehuda Ben-Zion, Robert Shcherbakov and an anonymous reviewer for very helpful recommendations. The Earthquake Commission Time Varying Hazard Programme provided financial support through project 14/TV682.

REFERENCES

- Atkinson, B. K., 1984. Subcritical crack growth in geological materials, *J. Geophys. Res.*, **89**, 4077–4114.
- Catalli, F., Cocco, M., Console, R. & Chiaraluce, L., 2008. Modeling seismicity rate changes during the 1997 Umbria-Marche sequence (central Italy) through rate- and state-dependent model, *J. Geophys. Res.*, **113**, B11301.
- Cocco, M., Hainzl, S., Catalli, F., Enescu, B., Lombardi, A.M. & Woessner, J., 2010. Sensitivity study of forecasted aftershock seismicity based on Coulomb stress calculation and rate- and state-dependent frictional response, *J. Geophys. Res.*, **115**, B05307, doi: 10.1029/2009JB006838.
- Dieterich, J. H., 1994. A constitutive law for rate of earthquake production and its application to earthquake clustering, *J. Geophys. Res.*, **99**, 2,601–2,618.
- Dieterich, J. H., Cayol, V. & Okubo, P., 2000. The use of earthquake rate changes as a stress meter at Kilauea volcano, *Nature*, **408**, 457–460.
- Gerstenberger, M. C. & Rhoades, D. A., 2010. New Zealand earthquake forecast testing centre, *Pure and Applied Geophysics*, **167**(8/9), 877–892, doi:10.1007/s00024-010-0082-4.
- Hainzl, S., Brietzke, G. B. & Zöller, G., 2010. Quantitative earthquake forecasts resulting from static stress triggering, *J. Geophys. Res.*, **115**, B11311, doi: 10.1029/2010JB007473.

- Hainzl, S., Zakharov, O. & Marsan, D., 2013. Impact of aseismic transients on the estimation of productivity parameters, *Bull. Seism. Soc. Am.*, **103**, 1723–1732.
- Hainzl, S., Moradpour, J. & Davidsen, J., 2014. Static stress triggering explains the empirical aftershock distance decay, *Geophys. Res. Lett.*, **41**, doi:10.1002/2014GL061975.
- Harte, D. S., 2013. Bias in fitting the ETAS model: a case study based on New Zealand seismicity, *Geophys. J. Int.*, **192**, 390–412.
- Harte, D. S., 2015. Model parameter estimation bias induced by earthquake magnitude cutoff, *Geophys. J. Int.*, in press, doi: 10.1093/gji/ggv524.
- Hauksson, E., Yang, W. & Shearer, P., 2012. Waveform relocated earthquake catalog for southern California (1981 to 2011), *Bull. Seism. Soc. Am.*, **102**, 2239.
- Helmstetter, A., Kagan, Y. Y. & Jackson, D. D., 2005. Importance of small earthquakes for stress transfer and earthquake triggering, *J. Geophys. Res.*, **110**, B05S08.
- Helmstetter, A. & Shaw, B. E., 2006. Relation between stress heterogeneity and aftershock rate in the rate-and-state model, *J. Geophys. Res.*, **111**, B07304, doi:10.1029/2005JB004077.
- Helmstetter, A. & Sornette, D., 2002. Subcritical and supercritical regimes in epidemic models of earthquake aftershocks, *J. Geophys. Res.*, **107**(B10), 2237.
- Helmstetter, A., Kagan, Y. Y. & Jackson, D. D., 2006. Comparison of short-term and time-independent earthquake forecast models for southern California, *Bull. Seismol. Soc. Am.*, **96**(1), 90–106.
- Holschneider, M., Narteau, C., Shebalin, P., Peng, Z. & Schorlemmer, D., 2012. Bayesian analysis of the modified Omori law, *J. Geophys. Res.*, **117**, B06317, doi:10.1029/2011JB009054.
- Kagan, Y. Y., 2004. Short-term properties of earthquake catalogs and models of earthquake source, *Bull. Seismol. Soc. Am.*, **94**(4), 1207–1228.
- Kostrov, V. V., 1974. Seismic moment and energy of earthquakes, and seismic flow of rock, *Earth Phys.*, **1**, 23–40.
- Lee, W. H. K. & Stewart, S. W., 1989. Large-scale processing and analysis of digital waveform data from the USGS Central California microearthquake network, In: Litehiser, J.J. (Ed.), *Observatory Seismology: An Anniversary Symposium on the Occasion of the Centennial of the University of California at Berkeley Seismographic Stations*. University of California Press. p. 86.
- Moradpour, J., Hainzl, S. & Davidsen, J. 2014. Non-trivial decay of aftershock density with distance in southern California, *J. Geophys. Res.*, doi: 10.1002/2014JB010940.
- Narteau, C., Shebalin, P. & Holschneider, M., 2002. Temporal limits of the power law aftershock decay rate, *J. Geophys. Res.*, **107**(B12), 2359, doi:10.1029/2002JB001868.
- Ogata, Y., 1988. Statistical models for earthquake occurrence and residual analysis for point processes, *J. Am. Stat. Assoc.*, **83**, 9–27.
- Press, W. H., Teukolsky, S. A., Vetterling, W. T. & Flannery, B. P., 1992. *Numerical Recipes in C: The Art of Scientific Computing*, Second Edition, Cambridge University Press.
- Rhoades, D. A., 2013. Mixture models for improved earthquake forecasting with short-to-medium time horizons, *Bull. Seismol. Soc. Am.*, **103**, 2203–2215.
- Scholz, C., 1968. The frequency-magnitude relation of microfracturing in rocks and its relation to earthquakes, *Bull. Seismol. Soc. Am.*, **58**, 399–415.
- Shcherbakov, R., Yakovlev, G., Turcotte, D. L. & Rundle, J. B., 2005. Model for the distribution of aftershock interoccurrence times, *Phys. Rev. Lett.*, **95**, 218501.
- Sornette, D. & Werner, M. J., 2005. Constraints on the size of the smallest triggering earthquake from the epidemic-type aftershock sequence model, Bath's law, and observed aftershock sequences, *J. Geophys. Res.*, **110**, doi:10.1029/2004JB003535.
- Stein, S. & Liu, M., 2009. Long aftershock sequences within continents and implications for earthquake hazard assessment, *Nature*, **462**, doi:10.1038/nature08502.
- Tahir, M., Grasso, J.-R. & Amorèse, D., 2012. The largest aftershock: How strong, how far away, how delayed? *Geophys. Res. Lett.*, **39**, L04301.
- Utsu, T., Ogata, Y. & Matsu'ura, R. S., 1995. The centenary of the Omori formula for a decay of aftershock activity, *J. Phys. Earth*, **43**, 1–33.
- van Stiphout, T., Zhuang, J. & Marsan, D., 2012. Seismicity declustering, *Community Online Resource for Statistical Seismicity Analysis*, doi:10.5078/corssa-52382934. Available at <http://www.corssa.org>.
- Wells, D. L. & Coppersmith, K. J., 1994. New empirical relationships among magnitude, rupture length, rupture width, rupture area, and surface displacement, *Bull. Seismol. Soc. Am.*, **84**, 974–1002.
- Zhuang, J., Werner, M. J. & Harte, D. S., 2013. Stability of earthquake clustering models: Criticality and branching ratios, *Phys. Rev. E*, **88**, 062109.

Figure 1. Parameter bias resulting from the false assumption of $T = \infty$ in the maximum likelihood estimation of modified ETAS simulations: The estimated values of (a) background rate μ , (b) c , (c) p , (d) K , and (e) α are shown by symbols, while the true values are marked by lines. In each plot, the results are shown for simulations of the modified ETAS model with different p - and T -values. Each box is drawn around the region between the 25% and 75% quantiles of the distribution of the estimated parameter, with a horizontal line at the median value. Whiskers extend from the minimum to the maximum value of the analysed 100 simulations in each case.

Figure 2. Maximum likelihood estimates of T for the clusters selected from California, New Zealand and global catalogues: (a) histogram and (b) scatter plot between the mainshock magnitude M and T .

Figure 3. Comparison of estimated ETAS parameters based on the standard model ($T = \infty$) with corresponding results for the modified model with maximum likelihood estimate of T for the clusters selected from California, New Zealand and global catalogues: The estimated values of (a) background rate μ , (b) c , (c) p , (d) K , and (e) α , where diagonal lines indicate the case that both estimates are equal.

Figure 4. Results for synthetic sequences of the modified ETAS model with (a) $T = 365$, (b) 1000, and (c) 10,000 days: The maximum log-likelihood estimates of T are marked by points as a function of the estimated background rate. The background colors refer to the stacked probability density functions of the estimates (approximated by lognormal distributions), where dark colours indicate constrained estimates. The true values of the simulations are shown by horizontal lines.

Figure 5. Estimated T -value for the empirical earthquake sequences (selected with $\tilde{D} = 3.0$) as a function of (a) the estimated background rate of $M \geq M_{\min}$ events per day and (b) the estimated background rate density, defined as the number of $M \geq 0$ events per day and per km^2 . The symbols are in agreement with those in Fig. 2 and the background colours are calculated in the same way as for the synthetic sequences (see Fig. 3). The slope of the dashed line in (b) is consistent with $T \propto 1/\mu$.

Figure 6. Estimated apparent aftershock duration T_a as a function of background activity in the case of (a) modified ETAS simulations with mainshocks of different size and (b) observed sequences. The points and error bars in (a) indicate the median and the first and third quartile of the parameter distribution. The slopes of the two dashed grey lines are consistent with decays according to μ^{-1} and $\mu^{-1.2}$, while the horizontal grey line indicates the T -value of the ETAS simulations. Results are colour coded by the mainshock magnitude M in (b), where crosses indicate the results in the case that all parameters were fitted, and bullets indicate the results in the case that $p = 1$ is fixed during parameter inversion to reduce the parameter uncertainties.

Figure 7. Information gains (IG) relative to Poisson models at different times following a mainshock of $M = 6$ (a, b) and $M = 7$ (c, d) in the case of 10 different seismicity histories preceding the mainshock. The training data set consists of only 100 events in (a) and (c), and of 500 events in (b) and (d). Solid lines show the average IG-value over simulated target earthquake aftershock sequences, while dashed lines show the fraction of target sequences with positive IG-values (see scale on right vertical axis), indicating superior ETAS forecasts. The grey vertical bars enclose the 25% and 75% quantiles of the estimated apparent aftershock duration T_a (corresponding to the results shown in Fig. 6a for the given background rate and mainshock magnitude).

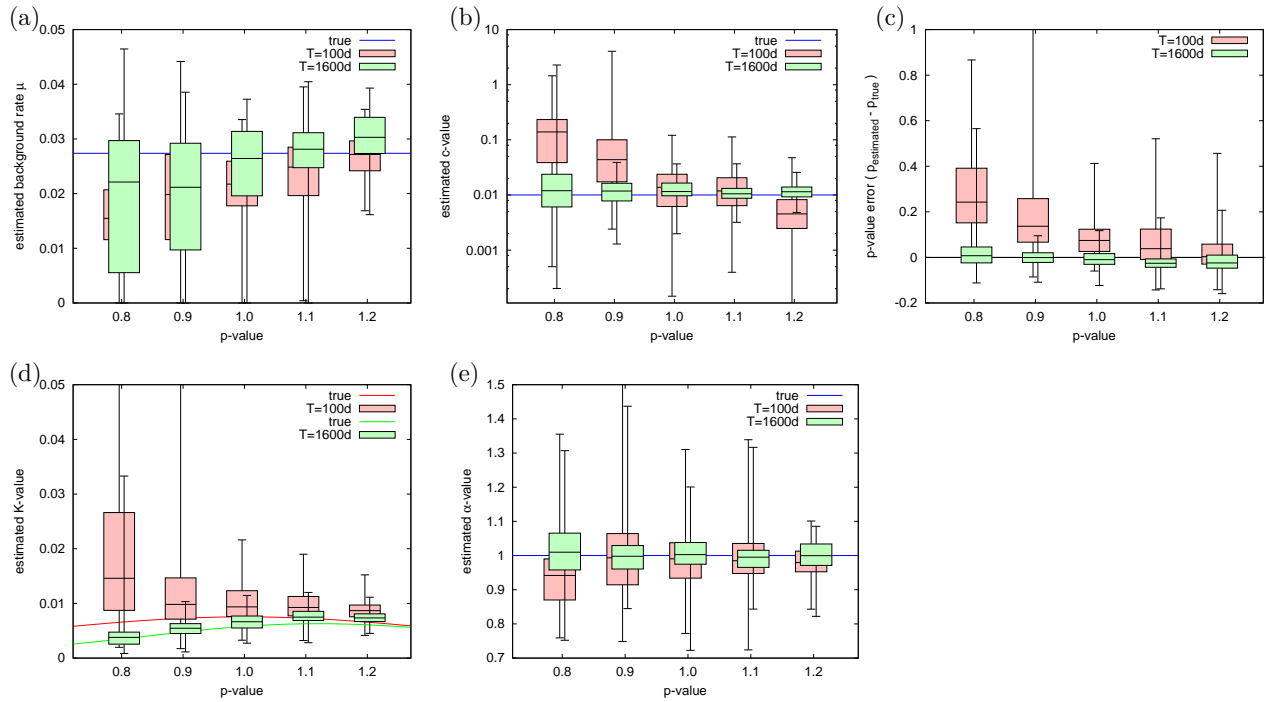


Figure 1. Parameter bias resulting from the false assumption of $T = \infty$ in the maximum likelihood estimation of modified ETAS simulations: The estimated values of (a) background rate μ , (b) c , (c) p , (d) K , and (e) α are shown by symbols, while the true values are marked by lines. In each plot, the results are shown for simulations of the modified ETAS model with different p - and T -values. Each box is drawn around the region between the 25% and 75% quantiles of the distribution of the estimated parameter, with a horizontal line at the median value. Whiskers extend from the minimum to the maximum value of the analysed 100 simulations in each case.

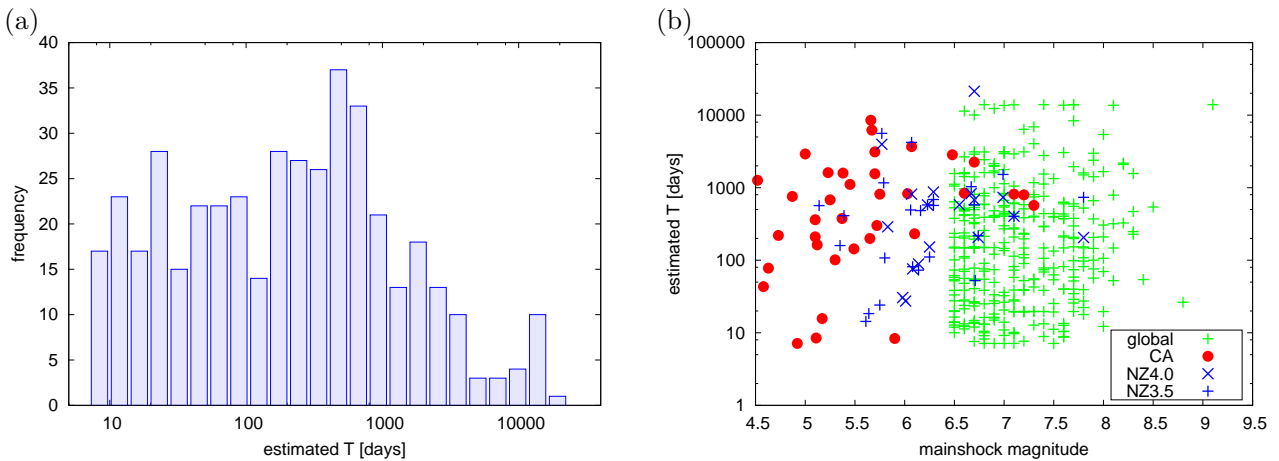


Figure 2. Maximum likelihood estimates of T for the clusters selected from California, New Zealand and global catalogues: (a) histogram and (b) scatter plot between the mainshock magnitude M and T .

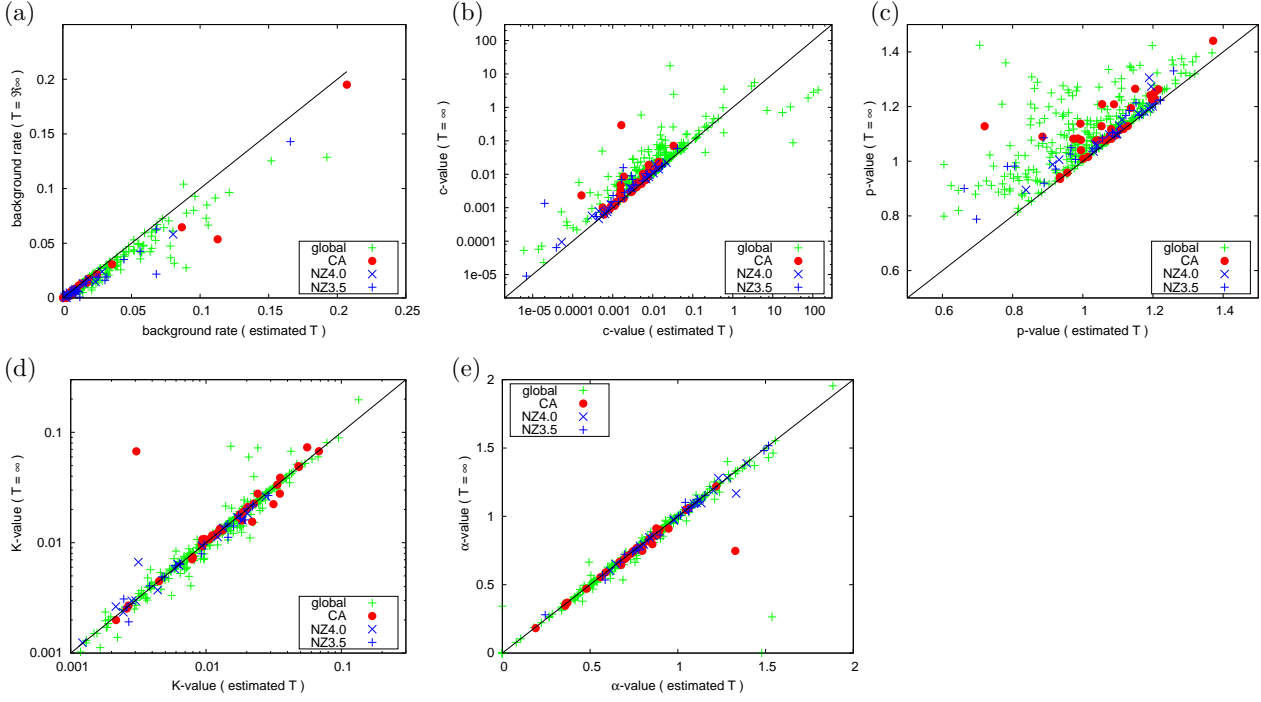


Figure 3. Comparison of estimated ETAS parameters based on the standard model ($T = \infty$) with corresponding results for the modified model with maximum likelihood estimate of T for the clusters selected from California, New Zealand and global catalogues: The estimated values of (a) background rate μ , (b) c , (c) p , (d) K , and (e) α , where diagonal lines indicate the case that both estimates are equal.

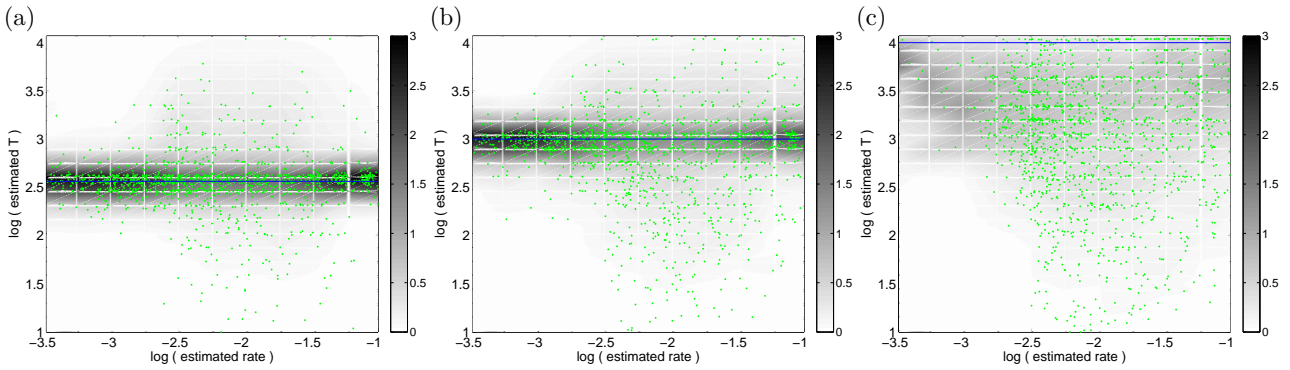


Figure 4. Results for synthetic sequences of the modified ETAS model with (a) $T = 365$, (b) 1000, and (c) 10,000 days: The maximum log-likelihood estimates of T are marked by points as a function of the estimated background rate. The background colors refer to the stacked probability density functions of the estimates (approximated by lognormal distributions), where dark colours indicate constrained estimates. The true values of the simulations are shown by horizontal lines.

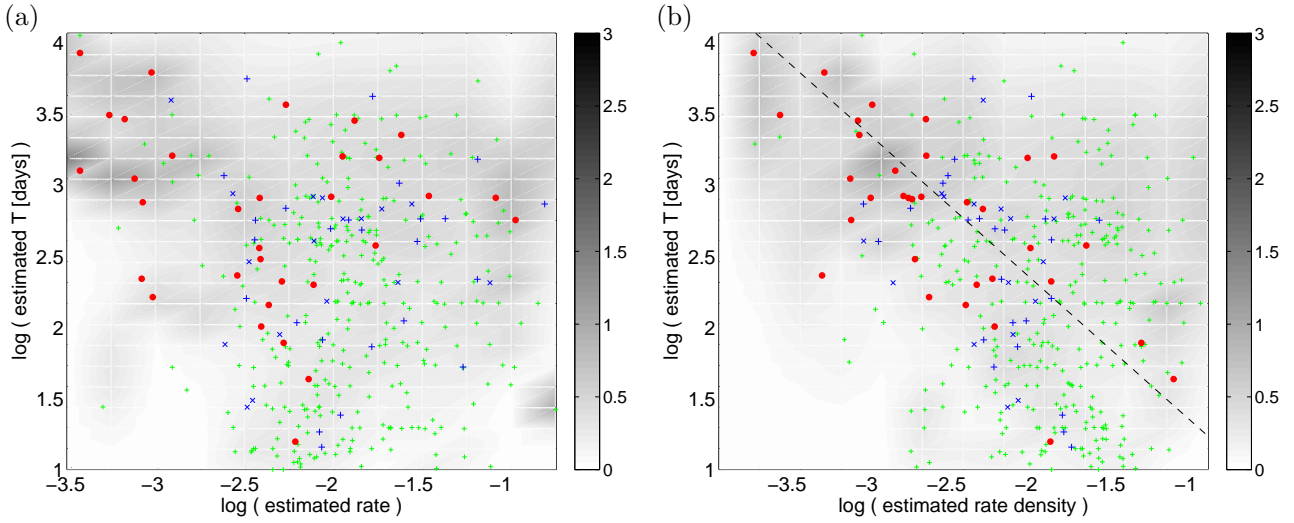


Figure 5. Estimated T -value for the empirical earthquake sequences (selected with $\tilde{D} = 3.0$) as a function of (a) the estimated background rate of $M \geq M_{\min}$ events per day and (b) the estimated background rate density, defined as the number of $M \geq 0$ events per day and per km^2 . The symbols are in agreement with those in Fig. 2 and the background colours are calculated in the same way as for the synthetic sequences (see Fig. 3). The slope of the dashed line in (b) is consistent with $T \propto 1/\mu$.

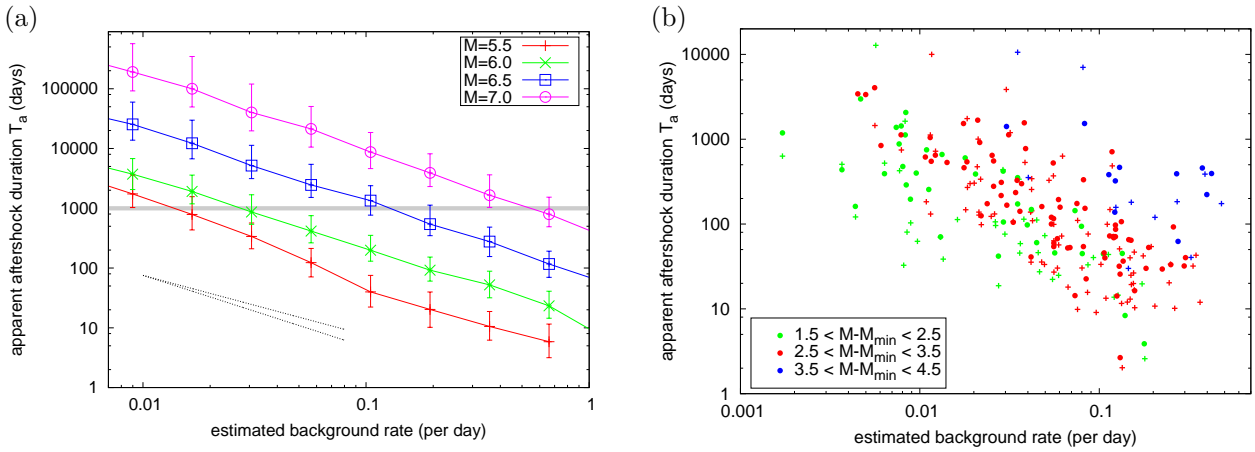


Figure 6. Estimated apparent aftershock duration T_a as a function of background activity in the case of (a) modified ETAS simulations with mainshocks of different size and (b) observed sequences. The points and error bars in (a) indicate the median and the first and third quartile of the parameter distribution. The slopes of the two dashed grey lines are consistent with decays according to μ^{-1} and $\mu^{-1.2}$, while the horizontal grey line indicates the T -value of the ETAS simulations. Results are colour coded by the mainshock magnitude M in (b), where crosses indicate the results in the case that all parameters were fitted, and bullets indicate the results in the case that $p = 1$ is fixed during parameter inversion to reduce the parameter uncertainties.

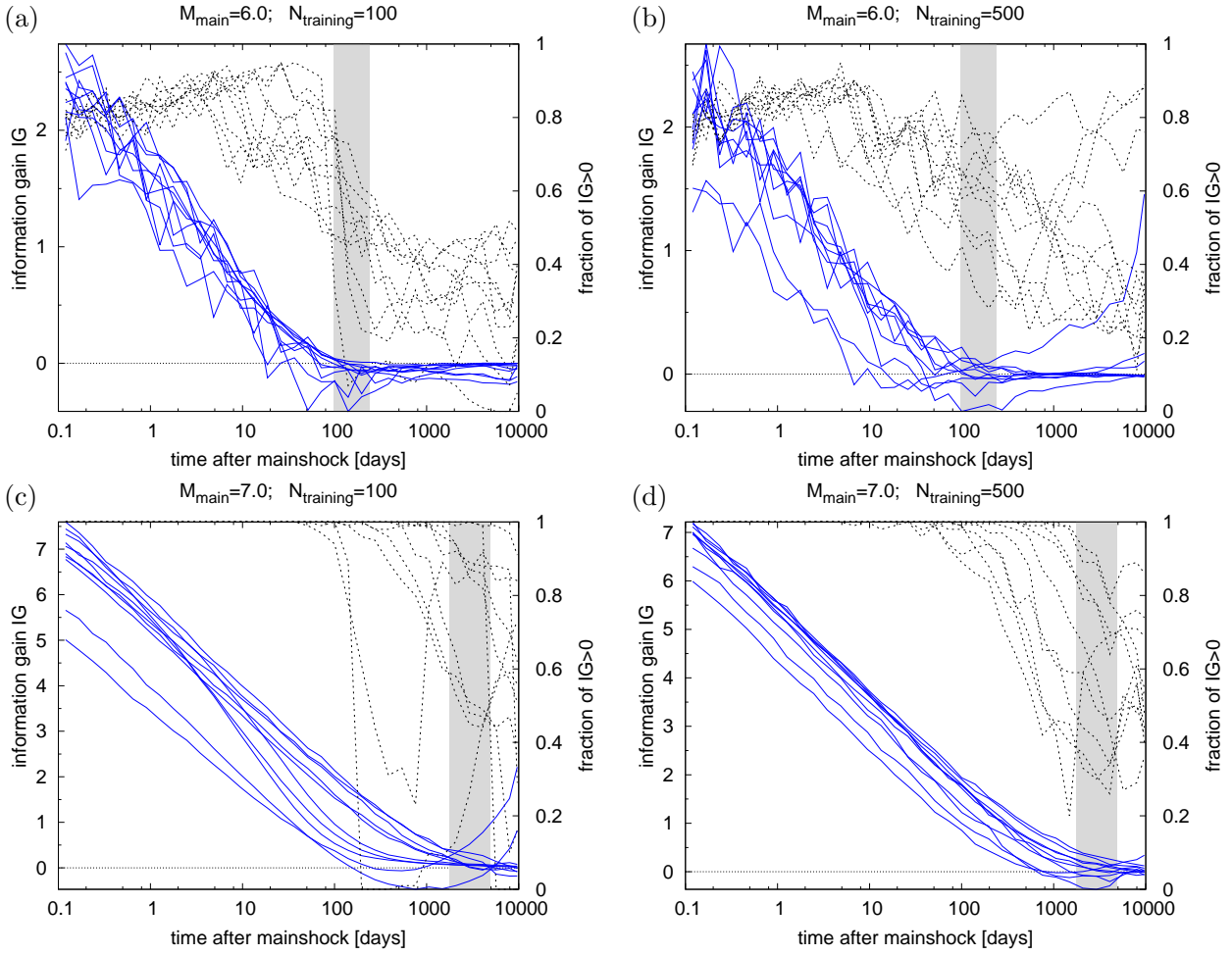


Figure 7. Information gains (IG) relative to Poisson models at different times following a mainshock of $M = 6$ (a, b) and $M = 7$ (c, d) in the case of 10 different seismicity histories preceding the mainshock. The training data set consists of only 100 events in (a) and (c), and of 500 events in (b) and (d). Solid lines show the average IG-value over simulated target earthquake aftershock sequences, while dashed lines show the fraction of target sequences with positive IG-values (see scale on right vertical axis), indicating superior ETAS forecasts. The grey vertical bars enclose the 25% and 75% quantiles of the estimated apparent aftershock duration T_a (corresponding to the results shown in Fig. 6a for the given background rate and mainshock magnitude).

Supplementary Material: Statistical estimation of the duration of aftershock sequences

S. Hainzl¹, A. Christophersen², D. Rhoades², D. Harte²

¹ GFZ German Research Centre for Geosciences, Potsdam, Germany (hainzl@gfz-potsdam.de)

² GNS Science, Lower Hutt, New Zealand

23 December 2015

SUMMARY

This material includes the results (Figs. S1-S4) corresponding to figures 2, 3, and 4 of main paper, but with smaller and larger spatial selection windows for cluster selection ($\tilde{D} = 1$ or 5). Furthermore, we present in Fig. S5 the results of manuscript Fig. 5b for rate densities which are transformed from the estimated rates with b -values individually estimated for each subregion, respectively sequence. Finally, Fig. S6 shows the uncertainties of the estimates of the triggering time T as functions of the background rate and mainshock magnitude.

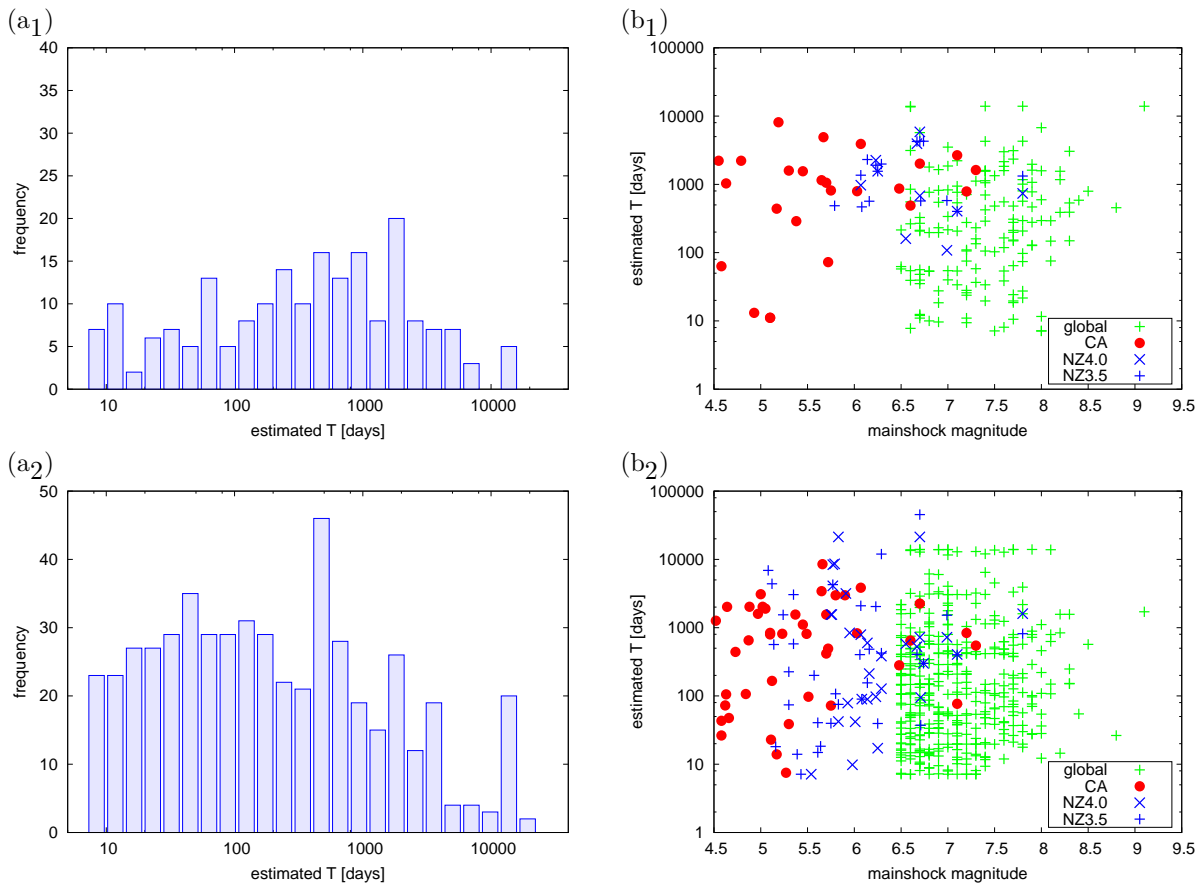


Figure 1. Maximum likelihood estimates of T for the clusters selected from California, New Zealand and global catalogues: (a_{1,2}) histogram and (b_{1,2}) scatter plot between the mainshock magnitude M and T in the case of $\tilde{D} = 1$ (a₁, b₁) and $\tilde{D} = 5$ (b₂, b₂). These results correspond to Fig. 2 of the main paper.

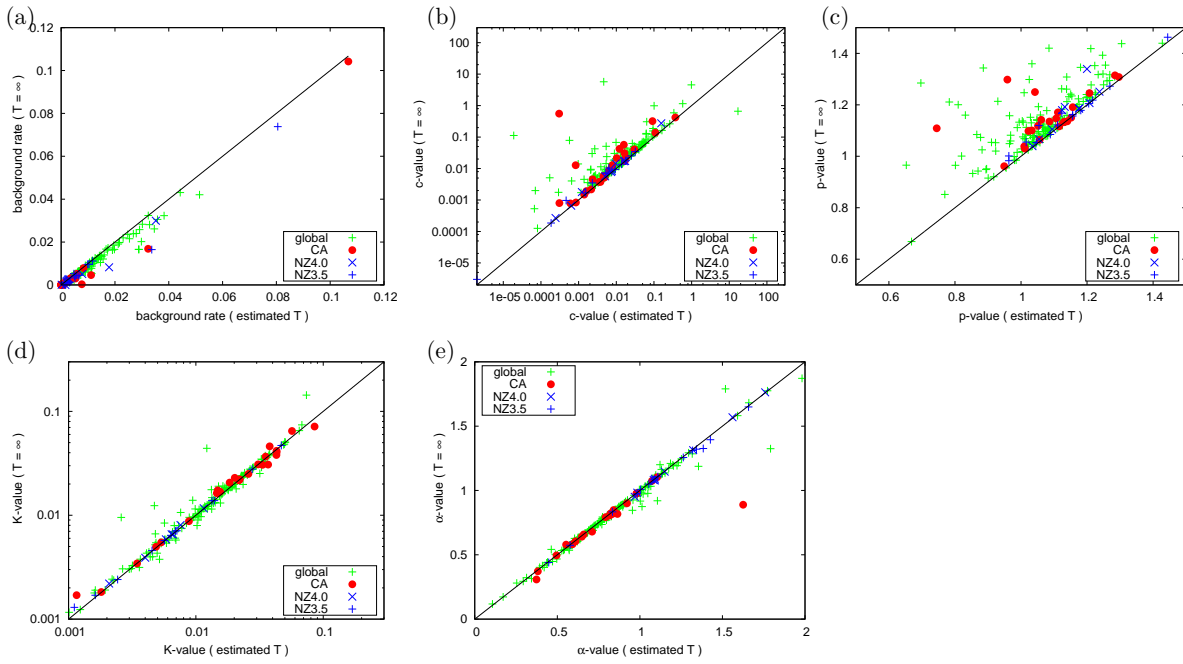


Figure 2. Comparison of estimated ETAS parameters based on the standard model ($T = \infty$) with corresponding results for maximum likelihood estimate of T in the case of a cluster selection with $\tilde{D} = 1$. For a detailed description of the plots, see Fig. 3 of the main paper.

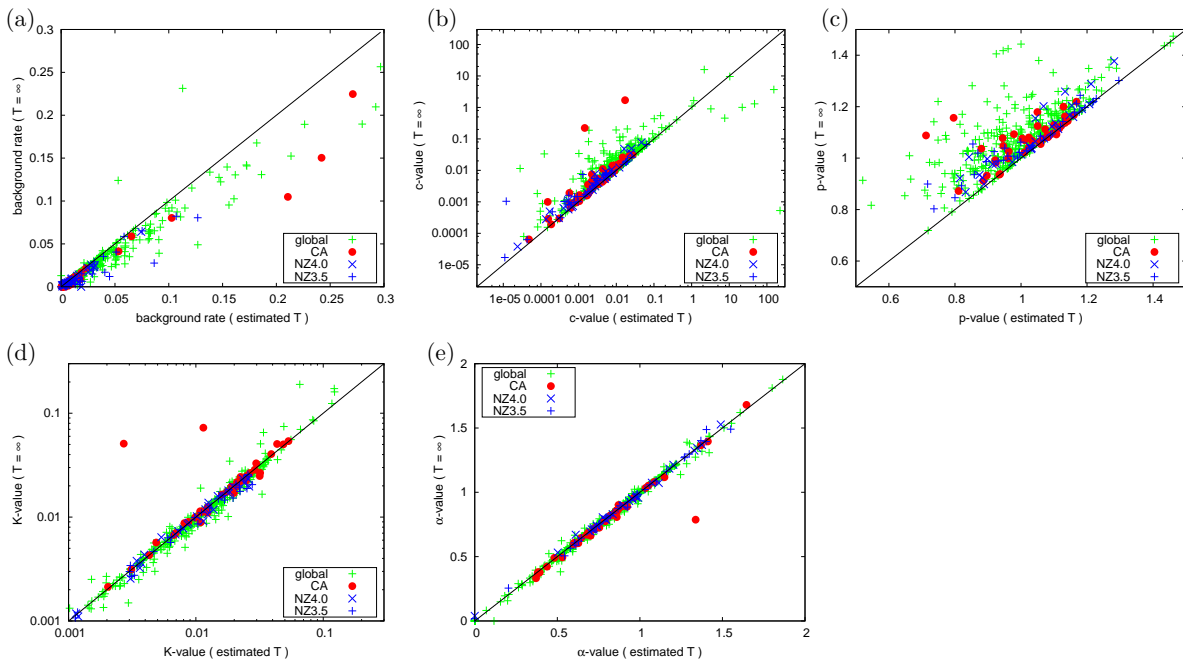


Figure 3. Same as Fig. S2 in the case of $\tilde{D} = 5$.

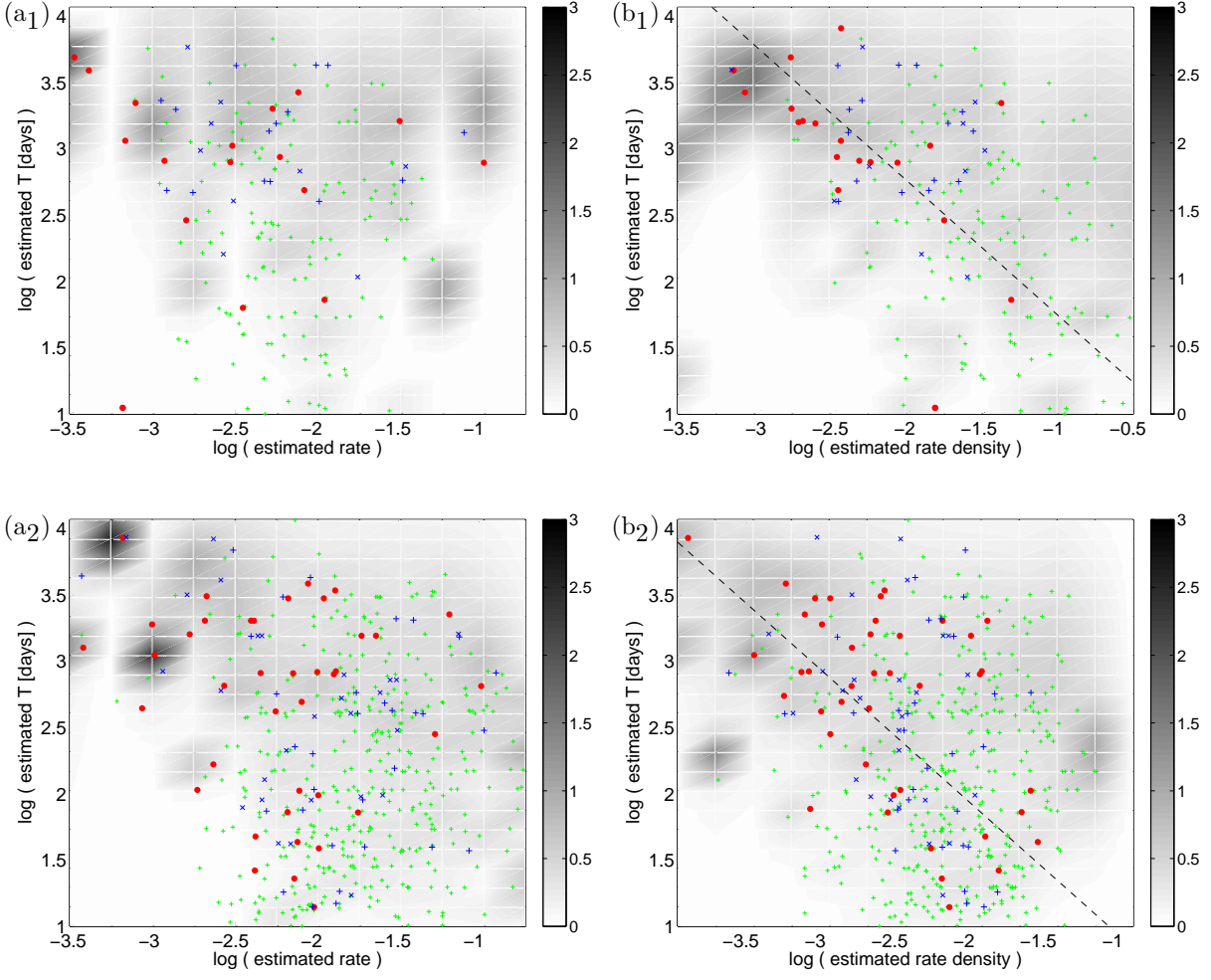


Figure 4. Same as manuscript-Fig. 5 in the case of clusters selected with $\tilde{D} = 1$ (plots a₁, b₁) or 5 (plots a₂, b₂): Estimated T -values for the empirical earthquake sequences as a function of (a_{1,2}) the estimated background rate of $M \geq M_{\min}$ events per day and (b_{1,2}) the estimated background rate density, defined as the number of $M \geq 0$ events per day and per km². See manuscript-Fig. 5 for more details.

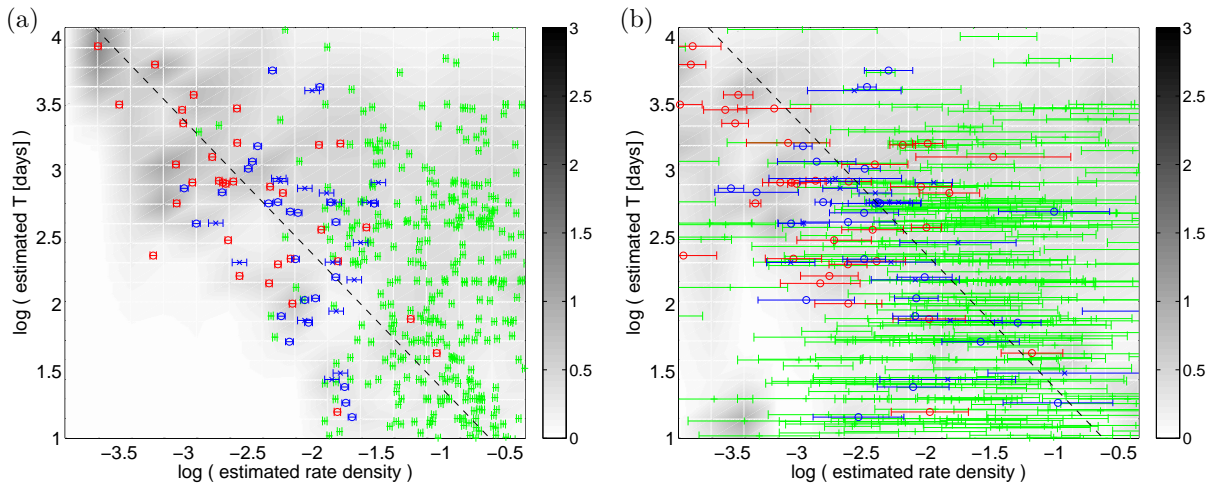


Figure 5. The results corresponding to Fig. 5b of the main paper in the case that the background rate density for $M \geq 0$ events (per day and per km²) is calculated (instead of $b = 1$) with (a) b -value estimated separately for each sub-catalog (global: $b = 1.162 \pm 0.004$, CA: $b = 1.013 \pm 0.008$, NZ4.0: $b = 1.07 \pm 0.014$, NZ3.5: $b = 1.006 \pm 0.009$), or (b) the b -value estimated for each sequence individually. Horizontal errors refer to the range of density estimates with b -value plus/minus one standard deviation.

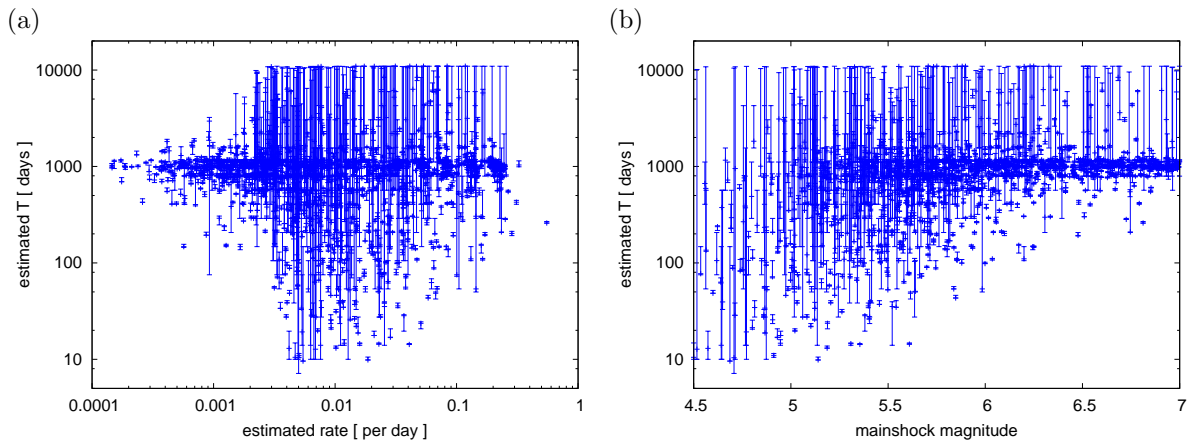


Figure 6. T -value estimations with their uncertainties in the case of synthetic sequences with $T = 1000$ days as a function of (a) the background rate and (b) the mainshock magnitude. Error bounds are related to the interval with Log-Likelihood values, $\mathcal{LL} \geq \mathcal{LL}_{max} - 0.5$ (corresponding to the 68% confidence interval in the case of a normal distribution). The results correspond to Fig.4b of the main manuscript, showing that the estimation is better constrained for larger mainshocks and lower background rates.



www.gns.cri.nz

Principal Location

1 Fairway Drive
Avalon
PO Box 30368
Lower Hutt
New Zealand
T +64-4-570 1444
F +64-4-570 4600

Other Locations

Dunedin Research Centre
764 Cumberland Street
Private Bag 1930
Dunedin
New Zealand
T +64-3-477 4050
F +64-3-477 5232

Wairakei Research Centre
114 Karetoto Road
Wairakei
Private Bag 2000, Taupo
New Zealand
T +64-7-374 8211
F +64-7-374 8199

National Isotope Centre
30 Gracefield Road
PO Box 31312
Lower Hutt
New Zealand
T +64-4-570 1444
F +64-4-570 4657